Memoirs of the Faculty of Engineering, Nagoya University
Vol. 36, No. 2 (1984)

STUDY ON STRESS DISTRIBUTION IN STRIP ROLLING

—— Rolling Pressure and Stresses at the Upper Stream Side of Roll Gap ——

YASUHISA TOZAWA and TAKASHI ISHIKAWA

Department of Iron and Steel Engineering

(Received October 31, 1984)

Abstract

An analysis for elastic deformation of rolls during rolling in four high mill is presented, in which the deformation of rolls is divided into three components; deflection of backup roll, deflection of work roll on an elastic foundation and flattening of work roll surface. And using this analysis the rolling force distribution is calculated from the contour of deformed roll obtained by experiment. Influence of rolling conditions on the distributions of rolling force and thickness across the strip width is investigated. On the other hand, the distribution of rolling pressure is directly measured by using multi-channelled pressure-sensor and the newly developed measuring system. The optimum condition for the pin method, which is adopted in measuring the pressure, is also discussed. Influence of rolling conditions on the distribution of rolling pressure is investigated and the results are compared with those calculated by using the analysis mentioned above. As another experimental approach, the distribution of stresses at the upper stream side of roll gap is measured under various rolling conditions and after comparison of the results with the calculated results by FEM, the distribution of stresses at the entry of roll gap is estimated.

CONTENTS

General Introduction

In the history of the rolling of strip, producing the strip with a close tolerance of thickness over the strip length was a main object. But now it has become easy becauce of the contribution of two-dimensional theory of rolling and the development of automatic gauge control system. And new requirements, flatness and crown of rolled strip, arise and recently requirement for edge-drop grows up in addition to crown. The flatness defect and the non-uniformity of thickness across the width are connected each other and both phenomena result from the same two reasons. One is that the deformation of the strip in the roll gap is not uniform across the width. The other is that the roll gap during rolling is not uniform along the roll barrel. The former is a problem of deformation of work material and the latter is that of rolls, and the rolling pressure acts at interface between the work material and the roll. Therefore the rolling pressure is one of the important informations for discussing the deformations of both of them.

There have been a lot of studies about the measurement of the distribution of rolling pressure. But a reliability of the obtained results, most of which are measured by the pin method, is not sufficient because the measuring system is poor and the discussion about the accuracy of the measuring method is not adequet. Moreover, the deformation of roll is not taken into consideration at all.

In this paper, the distribution of rolling pressure is not only measured directly but also calculated from the deformation of roll. Besides, the distribution of stresses at the upper stream side of roll gap is measured in order to estimate the stresses at the entry of roll gap. This study has been carried out at authors' laboratory together with many their colleagues.

Part 1 deals with the analysis to obtain the pressure distribution from the contour of deformed roll, and the influence of rolling condition on the distribution of rolling force and deflection of roll is investigated[1~4].

Part 2 deals with the measurement of distribution of rolling pressure by using multi-channelled pressure-sensor and a new data processing system, and many data are obtained for various rolling conditions[5~7].

Part 3 deals with the measurement of distribution of stresses at the upper stream side of roll gap, and the measured results are discussed by comparing with the calculated ones by FEM[8, 9].

Part 1. Analysis to Obtain the Pressure Distribution from the Contour of Deformed Roll

Yasuhisa TOZAWA, Masanobu UEDA, Tomoo KUMABE,
Masao NAKAMURA and Mikio SASANABE

1. 1. Introduction

In general, thickness of rolled strip is not uniform across the strip width and the non-uniformity is distinguished between edge-drop and strip crown. The technique of roll bending or thermal crown control is used in order to improve the non-uniformity of thickness, but producing the rolled strip without edge-drop is impossible

practically and the problem is how to decrease the edge-drop. The profile of rolled strip is determined by the contour of deformed roll, therefore it is necessary to know exactly how rolls deform during rolling. There are a lot of papers about the deformation of rolls. Emicke[10] and Larke et al.[11] calculated the roll deflection assuming roll as a simple beam. Hichcock[12], Fujisawa et al.[13] and Huggins et al.[14] calculated flattening of roll surface. Fazan[15] found the distribution of contact force between work roll and backup roll by the experiment. Stone et al.[16], Troost et al.[17] and Shiozaki[18] studied about the roll bending. In these papers, the distribution of rolling force across the strip width and its relation to the deflection of roll were not mentioned. As a matter of fact, rolling force doesn't distribute uniformly across the width.

In part 1, the analysis to obtain the distribution of rolling force from the contour of deformed roll is proposed and then by using this analysis and the contour of deformed roll measured, the influence of rolling condition on the distribution of rolling force and deflection of roll is investigated.

1. 2. Analysis for elastic deformation of rolls

Rolling force acting on the work roll causes several kinds of deformation in rolls.

In case of 4-high mill, the deformation of rolls by the rolling force is divided into the following three components[1, 4, 19].

(a) Deflection of backup roll (Fig. 1. 1(d))

(b) Deflection of work roll (Fig. 1. 1(b), (c)) (include compression between rolls)

(c) Flattening of work roll surface (Fig. 1. 1(a))

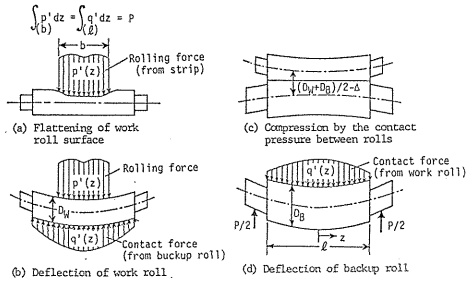

Fig. 1. 1 Elastic deformation of rolls in 4-high mill.

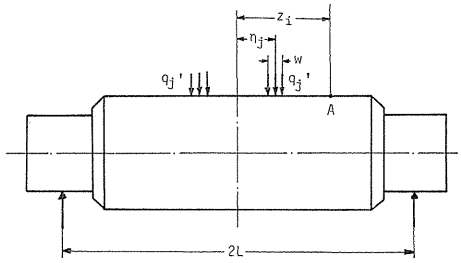

Fig. 1. 2 Notations used for analysis of deflection of backup roll.

1. 2. 1. Deflection of backup roll

When the force per unit width q_j' acts upon the finite width w at distance η_j from the centre as shown in Fig. 1. 2, the deflection of backup roll at a point A, which is distant z_i from the centre, is expressed as follows by considering roll as the simple beam, in which components not only by bending moment $(\delta_{Bb})_{ij}$ but also by shearing force $(\delta_{Bs})_{ij}$ are included.

For $z_i \leqq \eta_j$,

$$(\delta_{Bb})_{ij}=-\frac{q_j'wL^3}{6E_BI_B}\left[\left(1-\frac{z_i}{L}\right)^3-3\left(1+\frac{\eta_j}{L}\right)\left(1-\frac{\eta_j}{L}\right)\left(1-\frac{z_i}{L}\right)-\left\{\left(1-\frac{z_i}{L}\right)-\left(1-\frac{\eta_j}{L}\right)\right\}^3\right] \tag{1.1}$$

$$(\delta_{Bs})_{ij}=\frac{4q_j'w}{3A_BG_B}(L-\eta_j) \tag{1.2}$$

For $z_i>\eta_j$,

$$(\delta_{Bb})_{ij}=-\frac{q_j'wL^3}{6E_BI_B}\left\{\left(1-\frac{z_i}{L}\right)^3-3\left(1+\frac{\eta_j}{L}\right)\left(1-\frac{\eta_j}{L}\right)\left(1-\frac{z_i}{L}\right)\right\} \tag{1.3}$$

$$(\delta_{Bs})_{ij}=\frac{4q_j'w}{3A_BG_B}(L-z_i) \tag{1.4}$$

Therefore, total deflection of backup roll is

$$(\delta_B)_{ij}=(\delta_{Bb})_{ij}+(\delta_{Bs})_{ij} \tag{1.5}$$

And,

$$(\delta_B)_i=\sum_{j=1}^{m}\{(a_B)_{ij}\}q_j' \tag{1.6}$$

where

$$(a_B)_{ij}=-\frac{wL^3}{6E_BI_B}\left[\left(1-\frac{z_i}{L}\right)^3-3\left(1+\frac{\eta_j}{L}\right)\left(1-\frac{\eta_j}{L}\right)\left(1-\frac{z_i}{L}\right)-\left\{\left(1-\frac{z_i}{L}\right)-\left(1-\frac{\eta_j}{L}\right)\right\}^3\right]+\frac{4w}{3A_BG_B}(L-\eta_j)\ :\ \text{for } z_i\leq\eta_j$$

$$(a_B)_{ij}=-\frac{wL^3}{6E_BI_B}\left\{\left(1-\frac{z_i}{L}\right)^3-3\left(1+\frac{\eta_j}{L}\right)\left(1-\frac{\eta_j}{L}\right)\left(1-\frac{z_i}{L}\right)\right\}+\frac{4w}{3A_BG_B}(L-z_i)\ :\ \text{for } z_i>\eta_j$$

1. 2. 2. Deflection of work roll

For the case of contact of two cylinders (See Fig. 1. 1(c)), the change in the distance between their axes due to the local compression near the surface of contact is given by Hertz's equation[20].

$$\frac{1}{c}=\frac{d\Delta}{dq'}=\frac{E_R}{\pi}[0.118+ln(D_W+D_B)-lnE_R-lnq'] \tag{1.7}$$

where, $$E_R=\frac{1-\nu_W^2}{E_W}+\frac{1-\nu_B^2}{E_B}$$

According to this equation, the ratio of the contact force to the change in the distance varies little with increasing the contact force. Then the deflection of work roll is analyzed by considering as a finite beam rested on the elastic foundation of which elastic constant is determined by Eq. (1.7). In order to obtain the deflection of a finite beam on which force P_0 is acting symmetrically as shown in Fig. 1. 3 (a), the deflection of an infinite beam on which force (P_0, Q_0) or moment (M_0) acts as shown in Fig. 1. 3 (b), (c) and (d) is analyzed. If Q_0 and M_0 are determined to satisfy that the each sum of shearing force and moment at the point C and C′ is equal to zero, the sum of the deflections of three infinite beams shown in Fig. (b), (c) and (d) gives the deflection of a finite beam (Fig. (a)).

When concentrated force P_0 is acting on an infinite beam rested on the elastic foundation of which elastic constant is c as shown in Fig. 1. 4(a), we have following equations.

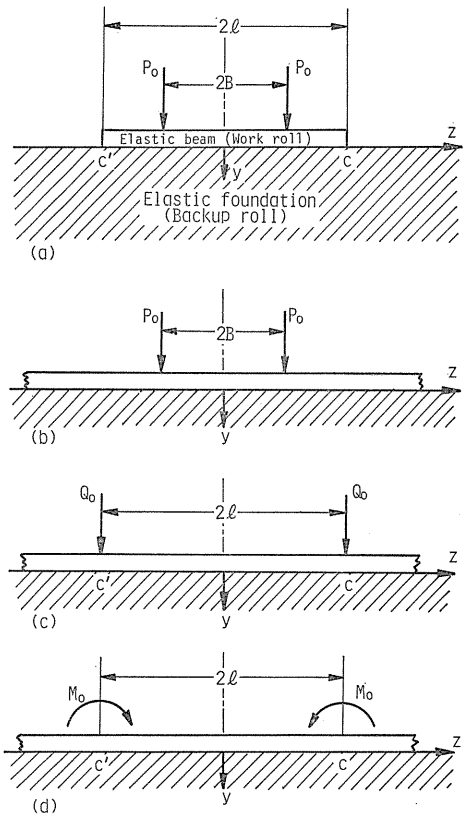

Fig. 1. 3 Work roll considered as a finite beam on the elastic foundation.

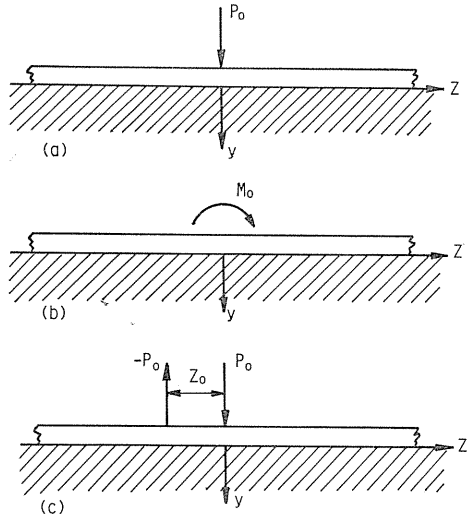

Fig. 1. 4 Infinite beam on the elastic foundation.

$$E_W I_W \frac{d^4 y_b}{dz^4} = -cy \tag{1.8}$$

$$A_W G_W \frac{d^2 y_s}{dz^2} = \frac{4}{3} cy \tag{1.9}$$

$$y_b+y_s=y \tag{1.10}$$

Shearing force V and moment M and then the deflection by bending moment y_b and that by shearing force y_s are obtained by solving the simultaneous differential equations (1.8) and (1.9).

$$y=\frac{P_0\beta}{2c\sqrt{1+\xi^2}}e^{-\kappa Z}\left(\cos\lambda Z+\frac{\kappa}{\lambda}\sin\lambda Z\right) \tag{1.11}$$

$$V=-\frac{P_0}{2}e^{-\kappa Z}\left\{\cos\lambda Z-\frac{1}{2}\left(1-\frac{\lambda^2}{\kappa^2}\right)\right\}\frac{\kappa}{\lambda}\sin\lambda Z \tag{1.12}$$

$$M=\frac{P_0}{4\beta\sqrt{1+\xi^2}}e^{-\kappa Z}\left(\cos\lambda Z-\frac{\kappa}{\lambda}\sin\lambda Z\right) \tag{1.13}$$

$$y_b=\frac{P_0\beta}{2c\sqrt{1+\xi^2}}\cdot\frac{1}{K_E{}^4}e^{-\kappa Z}\left\{(-5\kappa^4+10\kappa^2\lambda^2-\lambda^4)\right.$$
$$\left.\cos\lambda Z+(1-\kappa^4+10\kappa^2\lambda^2-5\lambda^4)\frac{\kappa}{\lambda}\sin\lambda Z\right\} \tag{1.14}$$

$$y_s=\frac{P_0\beta}{2c\sqrt{1+\xi^2}}\cdot\frac{K_G{}^2}{K_E{}^4}e^{-\kappa Z}\left\{(3\kappa^2-\lambda^2)\cos\lambda Z\right.$$
$$\left.+(\kappa^2-3\lambda^2)\frac{\kappa}{\lambda}\sin\lambda Z\right\} \tag{1.15}$$

where,

$$\left.\begin{aligned} &K_G{}^2=\frac{4c}{3A_WG_W},\quad K_E{}^4=\frac{c}{E_WI_W}\\ &\kappa=\beta\sqrt{1+\xi^2},\quad \lambda=\beta\sqrt{1-\xi^2}\\ &\beta=\frac{K_E}{\sqrt{2}},\quad \xi^2=\frac{K_G{}^2}{2K_E{}^2}\end{aligned}\right\} \tag{1.16}$$

Each deflection of beam shown in Fig. 1. 3(b), (c) is obtained as follows by use of the results just mentioned.

In case of Fig. 1. 3(b), the total deflection is

$$y_1=\frac{P_0\beta}{2c\sqrt{1+\xi^2}}\{\theta(|B-z|)+\theta(B+z)+\zeta(|B-z|)+\zeta(B+z)\} \tag{1.17}$$

where

$$\left.\begin{aligned} &\theta(Z)=e^{-\kappa Z}\cos\lambda Z\\ &\zeta(Z)=\frac{\kappa}{\lambda}\cdot e^{-\kappa Z}\sin\lambda Z\end{aligned}\right\} \tag{1.18}$$

The deflection by shearing force is

$$y_{s1}=\frac{P_0\beta}{2c\sqrt{1+\xi^2}}\cdot\frac{K_G{}^2}{K_E{}^4}[(3\kappa^2-\lambda^2)\{\theta(|B-z|)+\theta(B+z)\}$$
$$+(\kappa^2-3\lambda^2)\{\zeta(|B-z|)+\zeta(B+z)\}] \tag{1.19}$$

The deflection by bending moment is

$$y_{b1}=y_1-y_{s1} \tag{1.20}$$

In case of Fig. 1. 3(c), each deflection is obtain by the same manner.

$$y_2=\frac{Q_0\beta}{2c\sqrt{1+\xi^2}}\{\theta(l-z)+\theta(l+z)+\zeta(l-z)+\theta(l+z)\} \tag{1.21}$$

$$y_{s2}=\frac{Q_0\beta}{2c\sqrt{1+\xi^2}}\cdot\frac{K_G{}^2}{K_E{}^4}[(3\kappa^2-\lambda^2)\{\theta(l-z)+\theta(l+z)\}$$
$$+(\kappa^2-3\lambda^2)\{\zeta(l-z)+\zeta(l+z)\}] \tag{1.22}$$

$$y_{b2}=y_2-y_{s2} \tag{1.23}$$

To obtain the deflection y, shearing force V and moment M in an infinite beam on which moment M_0 is acting as shown in Fig. 1. 4(b), the deflection of a beam, on which force P_0 is acting conversely at two points of which distance is Z_0 (See Fig. 1. 4(c)), is determined and then Z_0 is brought closer to zero in this result.

$$y=\frac{M_0\beta^2}{c(1+\xi^2)}\cdot\frac{\kappa}{\lambda}e^{-\kappa Z}\sin\lambda Z \tag{1.24}$$

$$V=-\frac{M_0\beta(1+2\xi^2)}{2\sqrt{1+\xi^2}}e^{-\kappa Z}\left\{\cos\lambda Z+\frac{1-2\xi^2}{1+2\xi^2}\cdot\frac{\kappa}{\lambda}\sin\lambda Z\right\} \tag{1.25}$$

$$M=\frac{M_0}{2}e^{-\kappa Z}\left\{\cos\lambda Z-\frac{1-(\lambda/\kappa)^2}{2}\cdot\frac{\kappa}{\lambda}\sin\lambda Z\right\} \tag{1.26}$$

The deflection by shearing force and that by bending moment are

$$y_s=\frac{M_0\beta^2}{c}\cdot\frac{K_G{}^2}{K_E{}^2}e^{-\kappa Z}\left\{\cos\lambda Z+\frac{1-(\lambda/\kappa)^2}{2}\cdot\frac{\kappa}{\lambda}\sin\lambda Z\right\} \tag{1.27}$$

$$y_b=y-y_s \tag{1.28}$$

In case of Fig. 1. 3(d), each deflection is obtained as follows by use of these results.

$$y_3=\frac{M_0\beta^2}{c}\cdot\frac{1}{1+\xi^2}\{\zeta(l-z)+\zeta(l+z)\} \tag{1.29}$$

$$y_{s3}=\frac{M_0\beta^2}{c}\cdot 2\xi^2[\theta(l-z)+\theta(l+z)$$

$$+\frac{1-(\lambda/\kappa)^2}{2}\{\zeta(l-z)+\zeta(l+z)\}] \tag{1.30}$$

$$y_{b3}=y_3-y_{s3} \tag{1.31}$$

On the other hand, moment M and shearing force V at point C in Fig. 1. 3 is as follows.

In case of Fig. (b),

$$M_1=\frac{P_0}{4\beta\sqrt{1+\xi^2}}\{\theta(l-B)+\theta(l+B)-\zeta(l-B)-\zeta(l+B)\} \tag{1.32}$$

$$V_1=-\frac{P_0}{2}[\theta(l-B)+\theta(l+B)-\frac{1-(\lambda/\kappa)^2}{2}\{\zeta(l-B)+\zeta(l+B)\}] \tag{1.33}$$

In case of Fig. (c),

$$M_2=\frac{Q_0}{4\beta\sqrt{1+\xi^2}}\{1+\theta(2l)-\zeta(2l)\} \tag{1.34}$$

$$V_2=\frac{Q_0}{2}\left\{1-\theta(2l)+\frac{1-(\lambda/\kappa)^2}{2}\cdot\zeta(2l)\right\} \tag{1.35}$$

In case of Fig. (d),

$$M_3=\frac{M_0}{2}\left\{1+\theta(2l)-\frac{1-(\lambda/\kappa)^2}{2}\cdot\zeta(2l)\right\} \tag{1.36}$$

$$V_3=\frac{M_0\beta(1+2\xi^2)}{2\sqrt{1+\xi^2}}\left\{1-\theta(2l)-\frac{1-2\xi^2}{1+2\xi^2}\cdot\zeta(2l)\right\} \tag{1.37}$$

Then, both moment and shearing force at point C in Fig. (a) are zero, so

$$M_1+M_2+M_3=0 \tag{1.38}$$

$$V_1+V_2+V_3=0 \tag{1.39}$$

M_0 and Q_0 is obtained by solving above equations. Therefore, the total deflection y, the deflection by shearing force y_s and that by bending moment y_b are

$$y=y_1+y_2+y_3 \tag{1.40}$$

$$y_{s1}=y_{s1}+y_{s2}+y_{s3} \tag{1.41}$$

$$y_b=y_{b1}+y_{b2}+y_{b3}=y-y_s \tag{1.42}$$

By substituting η_j for B, z_i for z and $p'w$ for P_0 in these equations, the total deflection $(\delta_W)_{ij}$, the deflection by shearing force $(\delta_{Ws})_{ij}$ and that by bending moment $(\delta_{Wb})_{ij}$ are obtained from y, y_s and y_b respectively.

The final expression for the total deflection is as follows.

$$(\delta_W)_{ij}=\frac{p_j'w\beta}{2c\sqrt{1+\xi^2}}\{\theta(|\eta_j-z_i|)+\theta(\eta_j+z_i)+\zeta(|\eta_j-z_i|)+\zeta(\eta_j+z_i)\}$$

$$+\frac{p_j' w\beta Q_0}{2c\sqrt{1+\xi^2}}\{\theta(l-z_i)+\theta(l+z_i)+\zeta(l-z_1)+\zeta(l+z_i)\}$$

$$+\frac{p_j' w\beta^2 M_0}{c}\cdot\frac{1}{1+\xi^2}\{\zeta(l-z_i)+\zeta(l+z_i)\}$$

$$=(a_W)_{ij}\cdot p_j' \tag{1.43}$$

In this equation,

$$Q_0=\frac{1}{f}\left(\frac{eu-ft}{fv-gu}\cdot g-e\right),\quad M_0=\frac{eu-ft}{fv-gu} \tag{1.44}$$

$$e=\frac{1}{4\beta\sqrt{1+\xi^2}}\{\theta(l-\eta_j)+\theta(l+\eta_j)-\zeta(l-\eta_j)-\zeta(l+\eta_j)\} \tag{1.45}$$

$$f=\frac{1}{4\beta\sqrt{1+\xi^2}}\{1+\theta(2l)-\zeta(2l)\} \tag{1.46}$$

$$g=\frac{1}{2}\left\{1+\theta(2l)-\frac{1-(\lambda/\kappa)^2}{2}\cdot\zeta(2l)\right\} \tag{1.47}$$

$$t=-\frac{1}{2}\left[\theta(l-\eta_j)+\theta(l+\eta_j)-\frac{1-(\lambda/\kappa)^2}{2}\{\zeta(l-\eta_j)+\zeta(l+\eta_j)\}\right] \tag{1.48}$$

$$u=\frac{1}{2}\left\{\{1-\theta(2l)+\frac{1-(\lambda/\kappa)^2}{2}\cdot\zeta(2l)\right\} \tag{1.49}$$

$$v=\frac{1}{2\sqrt{1+\xi^2}}\left[(1+2\xi^2)\left\{1-\theta(2l)-\frac{1-2\xi^2}{1+2\xi^2}\cdot\zeta(2l)\right\}\right] \tag{1.50}$$

In general, the surface of the elastic foundation is not flat because of crown or deflection of backup roll.

When the gap δ_d exists between the beam and the foundation as shown in Fig. 1. 5, the deflection of work roll is obtained by adding the opposite deformation due to $\Delta q'$ $(=c\delta_d)$.

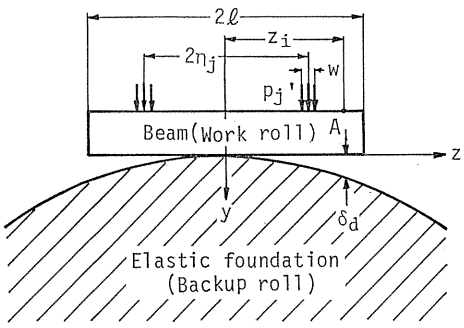

Fig. 1. 5 Work roll considered as a finite beam on the elastic foundation.

Therefore,

$$(\delta_W)_i=\sum_{j=1}^{n}\{(a_W)_{ij}\}p_j'-\sum_{j=1}^{m}\{(a_W)_{ij}\}\Delta q_j' \tag{1.51}$$

where $\Delta q_j' = c(\delta_d)_j$, $\delta_d = \delta_c + \delta_B - (\delta_B)_{z=0}$, δ_c is the crown of roll and δ_B is the deflection of backup roll expressed by Eq. (1.6).

1. 2. 3. Flattening of work roll surface

From the theory of elasticity[21], deformation at a point A on a surface of semi-infinite body by uniform pressure p $(=p_j'/l_d)$ distributed over CDEF (width w, length l_d) (Fig. 1.6) is given by

$$\delta_f = \frac{(1-\nu_W)^2 p}{\pi E_W} \int_0^{l_d} \int_{-w/2}^{w/2} \frac{dZdX}{s} \tag{1.52}$$

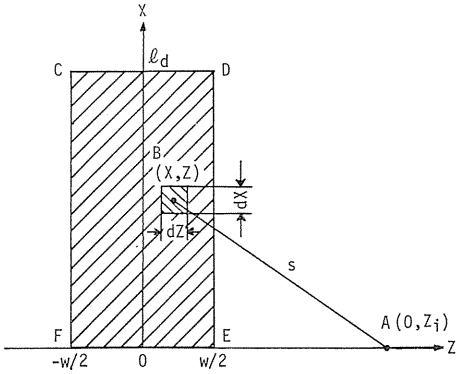

Fig. 1. 6 Notations used for analysis of deformation at a point A by uniform pressure p distributed over CDEF.

It is rewritten as

$$\delta_f = \frac{(1-\nu_W^2)p}{\pi E_W} \left\{ l_d \cdot ln \frac{\sqrt{l_d^2 + (Z_i + w/2)^2} + Z_i + w/2}{\sqrt{l_d^2 + (Z_i - w/2)^2} + Z_i - w/2} \right.$$
$$+ (Z_i + w/2) \cdot ln \frac{\sqrt{(Z_i + w/2)^2 + l_d^2} + l_d}{|Z_i + w/2|}$$
$$\left. - (Z_i - w/2) \cdot ln \frac{\sqrt{(Z_i - w/2)^2 + l_d^2} + l_d}{|Z_i - w/2|} \right\} \tag{1.53}$$

When the pressure acts on each area of the rectangles which is distant η_j symmetrically from the centre of roll barrel as shown in Fig. 1. 7 the flattening at the exit of roll gap is

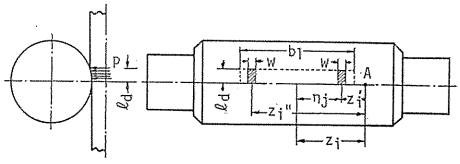

Fig. 1. 7 Notations used for analysis of roll flattening.

$$(\delta_f)_i = \sum_{j=1}^{n} \{(a_f)_{ij}\} p_j' \tag{1.54}$$

In the equation,

$$(a_f)_{ij}=-\frac{(1-\nu_W{}^2)}{\pi E_W}\left\{ln\frac{\sqrt{l_d{}^2+(z_i'+w/2)^2}+z_i'+w/2}{\sqrt{l_d{}^2+(z_i'-w/2)^2}+z_i'-w/2}\right.$$
$$+\frac{z_i'+w/2}{l_d}ln\frac{\sqrt{(z_i'+w/2)^2+l_d{}^2}+l_d}{|z_i'+w/2|}-\frac{z_i'-w/2}{l_d}ln\frac{\sqrt{(z_i'-w/2)^2+l_d{}^2}+l_d}{|z_i'-w/2|}$$
$$+ln\frac{\sqrt{l_d{}^2+(z_i''+w/2)^2}+z_i''+w/2}{\sqrt{l_d{}^2+(z_i''-w/2)^2}+z_i''-w/2}$$
$$\left.+\frac{z_i''+w/2}{l_d}ln\frac{\sqrt{(z_i''+w/2)^2+l_d{}^2}+l_d}{|z_i''+w/2|}-\frac{z_i''-w/2}{l_d}ln\frac{\sqrt{(z_i''-w/2)^2+l_d{}^2}+l_d}{|z_i''-w/2|}\right\} \tag{1.56}$$

where $z_i'=|z_i-\eta_j|$ and $z_i''=z_i+\eta_j$.
Therefore, the deflection of the roll at the exit of roll gap is expressed as

$$\begin{aligned}\delta_i&=(\delta_W)_i+(\delta_f)_i\\&=\sum_{j=1}^{n}\{(a_W)_{ij}+(a_f)_{ij}\}p_j'-c\sum_{j=1}^{m}\{(a_W)_{ij}\}(\delta_d)_j\end{aligned} \tag{1.57}$$

In case of 2-high mill, the deflection of roll δ_i is obtained as the sum of the deflection of backup roll expressed as Eq. (1.6), in which p_j', E_W, I_W, A_W and G_W are used instead of q_j', E_B, I_B, A_B and G_B respectively, and the flattening of roll surface (Eq. (1.54)).

$$\begin{aligned}\delta_i&=(\delta_B)_i+(\delta_f)_i\\&=\sum_{j=1}^{n}\{(a_B)_{ij}+(a_f)_{ij}\}p_j'\end{aligned} \tag{1.58}$$

The least squares approximate value of the rolling force p_j' at n regions across the strip width can be obtained by solving the simultaneous linear equations (Eq. (1.57) or Eq. (1.58)) numerically, when the total deformation of rolls δ_i are given at $m(\geq n+1)$ regions along the roll barrel. In case of 4-high mill, however, $(\delta_d)_j$ or $(\delta_B)_j$ is unknown, so the calculation starts with an initial value $(\delta_d)_j$ and the contact force q_i' is calculated as follows by use of obtained p_j'.

$$\begin{aligned}q_i'&=c\{(\delta_W)_i-(\delta_d)_i\}\\&=c\{(\delta_W)_i\}-c\{(\delta_c)_i+(\delta_B)_i-(\delta_B)_{i,\,z=0}\}\end{aligned} \tag{1.59}$$

Then, $(\delta_B)_i$ is calculated by substituting q_i' into Eq. (1.6) and by correcting $(\delta_d)_j$ the calculation is repeated until the convergency is obtained.

Finally, if p_j' is obtained, each component of roll deformation, the contact force between work roll and backup roll q_i' and total rolling force P_{cal} is calculated.

$$P_{cal}=2w\sum_{j=1}^{n}p_j' \tag{1.60}$$

1. 3. Experimental procedure

1. 3. 1. Method to measure the contour of elastically deformed roll

To measure the contour of roll during rolling, the same method as that of B. Fazan et al.[15] is adopted. A specimen is placed at the centre of roll barrel and some lead wires are arranged both side of specimen as shown in Fig. 1. 8 and they are rolled simultaneously. After rolling, thickness of strip and lead wires are measured. Fig. 1. 9 shows an example of the measured results of the thickness distribution of rolled strip and lead wires, which indicates the contour of deformed roll during rolling at the exit of roll gap, because the deformation of roll caused by rolling lead wires and elastic recovery of strip and lead is negligibly small.

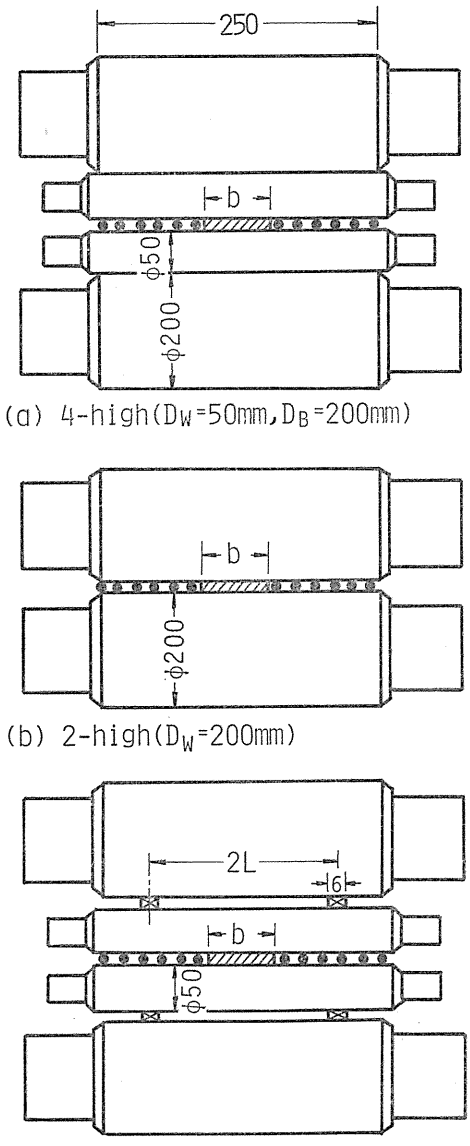

Fig. 1. 8 Methods for measuring the contour of elastically deformed roll during rolling and experimental conditions.

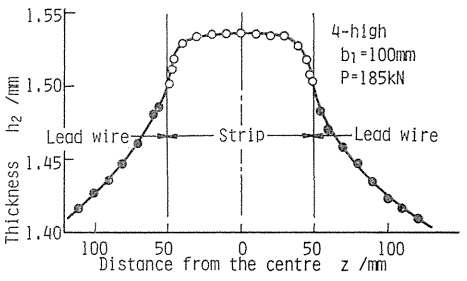

Fig. 1. 9 An example of the thickness distribution of rolled strip and lead wires.

Thickness of strip is measured by an electronic micrometer of which minimum reading is 0. 1 μm. A projector is used to measure the thickness of lead wire.

1. 3. 2. Rolling mill and specimen

Rolling mill used in the experiment is 2-high single stand mill having flat or crown rolls (of which lateral profile is

shown in Fig. 1. 10) 200 mm dia. of barrel length 250 mm and the mill is utilized as 4-high mill by inserting work rolls 50 mm dia..

Experiment is carried out on three kinds of roll condition as follows (Fig. 1. 8).

(a) 4-high (Dia. of work roll: D_W=50mm, Dia. of backup roll: D_B=200mm)

(b) 2-high (D_W=200mm)

(c) 2-high (D_W=50mm)

(i) $2L$=150mm

(ii) $2L$=200mm

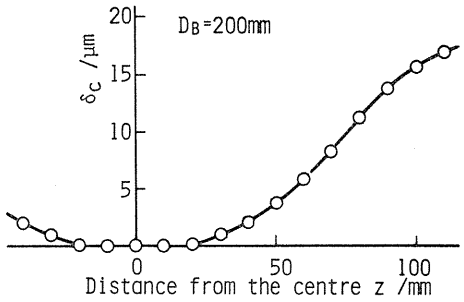

Fig. 1. 10 Lateral profile of backup roll with crown.

where, in case of (c) 2-high, strip is rolled in the special condition as shown in Fig. 1. 8(c) at which deflection of roll is larger than other cases.

Specimen used in the experiment is mild steel (SPCC) of 2. 0 mm in thickness and is finished to 25, 50, 100 or 150 mm in width by machining and then fully annealed.

Lead wires of 2. 0 mm and 2. 1 mm dia. are made from bilet of 20 mm dia. by extrusion.

Rolls are degreased with acetone prior to each experiment and strips are rolled under various kinds of reduction in thickness.

1. 4. Results

1. 4. 1. Examples of calculated results

Fig. 1. 11 shows some examples of calculated results. Influence of roll condition, strip width and roll crown on the results can be seen in Figs. (a)～(c), Figs.

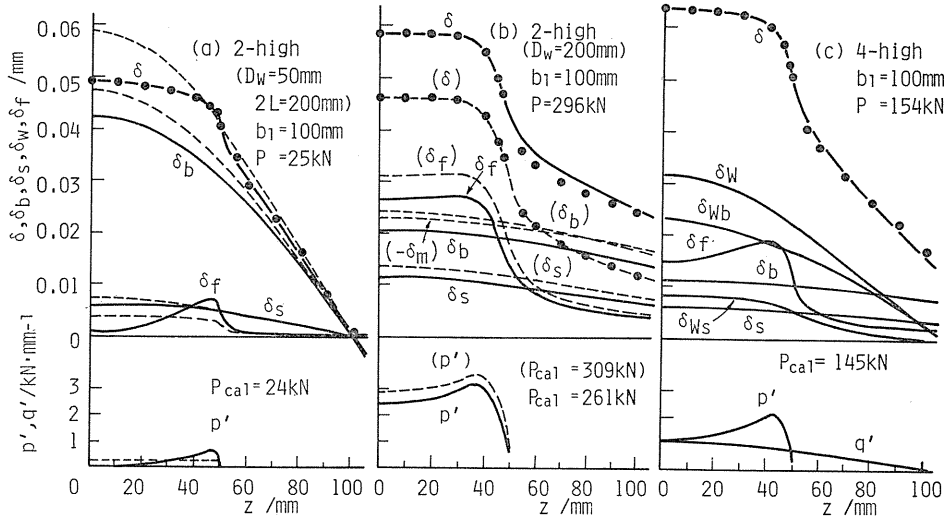

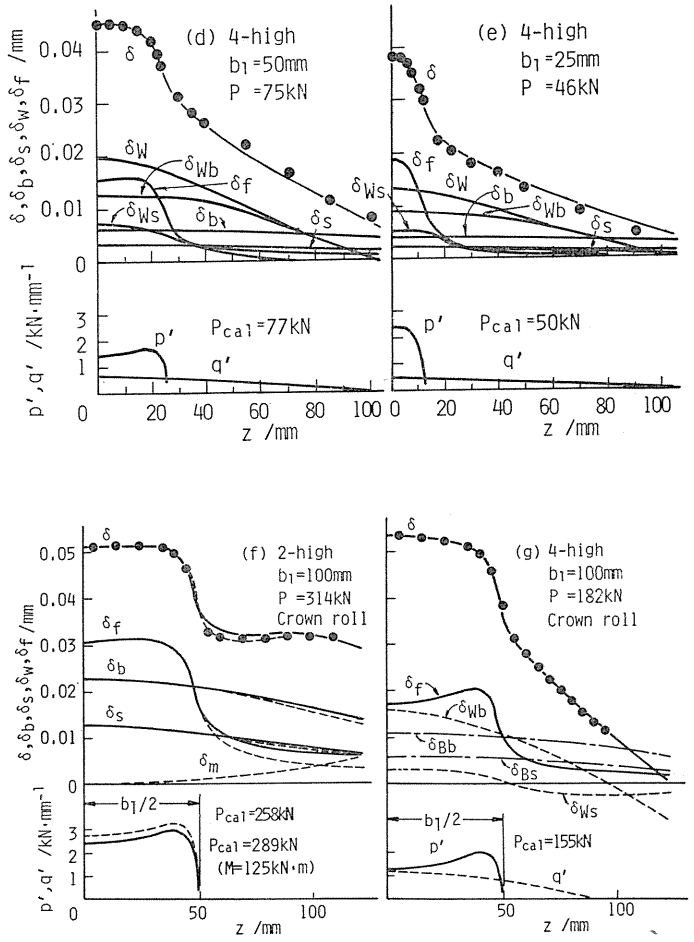

Fig. 1. 11 Distribution along the roll barrel of rolling force p', contact force q' between the rolls, total deformation of rolls δ, and each components of the deformation (δ_f: flatteinng, δ_b, δ_s: deflection by bending moment and shearing force, δ_{Wb}, δ_{Ws}: work roll deflection by bending moment and shearing force, $\delta_W=\delta_{Wb}+\delta_{Ws}$). (● : measured total deformation) (a) 2-high, ---: assuming that the rolling force p' is constant, $=P_{cal}/b_1$, (b) 2-high, ---: under the consideration of resistance moment M at the roll supports, δ_m: deflection by the resistance moment, (c), (d), (e) 4-high. (f) 2-high with crown roll, ---: under the consideration of resistance momens M at the roll suppors, δ_m: deflection by the resistance moment. (g) 4-high, with crown roll.

(d), (e) and Figs. (f), (g) respectively. Marks ● indicate the measured contour of deformed roll which are obtained from the difference between the thickness at the

centre and that at each position and they are plotted as the measured data coincides with the calculated result at the centre of roll barrel.

These results are summerized as follows.

1) In all cases, the rolling force per unit width p' isn't uniform across the strip width and the pattern of the distribution changes with rolling condition. For example, in case of narrow strip (Fig. (e)), the rolling force becomes maximum at the centre but in other cases, it becomes maximumn near the edge of strip. The contact force between work roll and backup roll q' is maximum at the centre and decreases gradually towards the edge of roll barrel like as parabola.

2) The distribution of calculated total deformation agrees well with the experimental one in case of 2-high (D_W=50mm) (Fig. (a)) and 4-high (Figs. (c), (d), (g)) but in other cases, there is a little difference between them at the region where strip doesn't contact with rolls.

3) The distribution of each component of deflection looks like parabola, and by the deflection a strip crown is produced.

4) In case of 4-high, the deflection of work roll $\delta_W(=\delta_{Wb}+\delta_{Ws})$ is large and as a result a strip crown is larger than that in case of 2-high.

5) Distribution of flattening of work roll surface δ_f is similar to the distribution of rolling force p' and it becomes maximum near the edge except for narrow strip, so it improves the strip crown. It is made clear that the distribution of δ_f depends strongly on that of p', by comparing with the result indicated by the broken lines in Fig. 1. 11(a) which is calculated on an assumption of uniform distribution of p'. As stiffness of roll in this case is very small, the difference can be seen in not only δ_f but δ_b and δ_s. In other cases of 2-high and 4-high, however, it is found that the distribution of deflection is almost determined only by total rolling force and not related to the distribution of rolling force per unit width.

1. 4. 2. Distribution of rolling force per unit width

The distributions of rolling force per unit width p' for various rolling conditions are summarized in Fig. 1. 12. Rolling force p' generally becomes maximum near the edge of strip. In each rolling condition, the position of maximum rolling force has tendency to move to the centre of strip when rolling force or reduction increases. Therefore, the distribution of rolling force for the condition of narrow strip (b_1=25mm, 50mm) changes from concave to convex with increase in rolling force (reduction). In comparison between 2-high and 4-high under the condition of same width and same rolling force, the position of maximum rolling force is almost same and the difference in rolling force between the maximum value of centre under the condition of 4-high is larger than that of 2-high.

In case of 2-high, the peak of rolling force near the edge under the condition of crown roll isn't so sharp as that under the condition of flat roll, but there is almost no difference in case of 4-high between the distribution of rolling force under the condition of crown roll and that of flat roll.

1. 4. 3. Each component of roll deformation

Fig. 1. 13 shows the relationship between calculated rolling force and each component of the roll deformation at centre of roll barrel.

In case of 4-high (Fig. (a)), δ_b, δ_s and δ_W are proportional to rolling force though δ_f isn't. δ_b and δ_s are hardly influenced with strip width and relatively

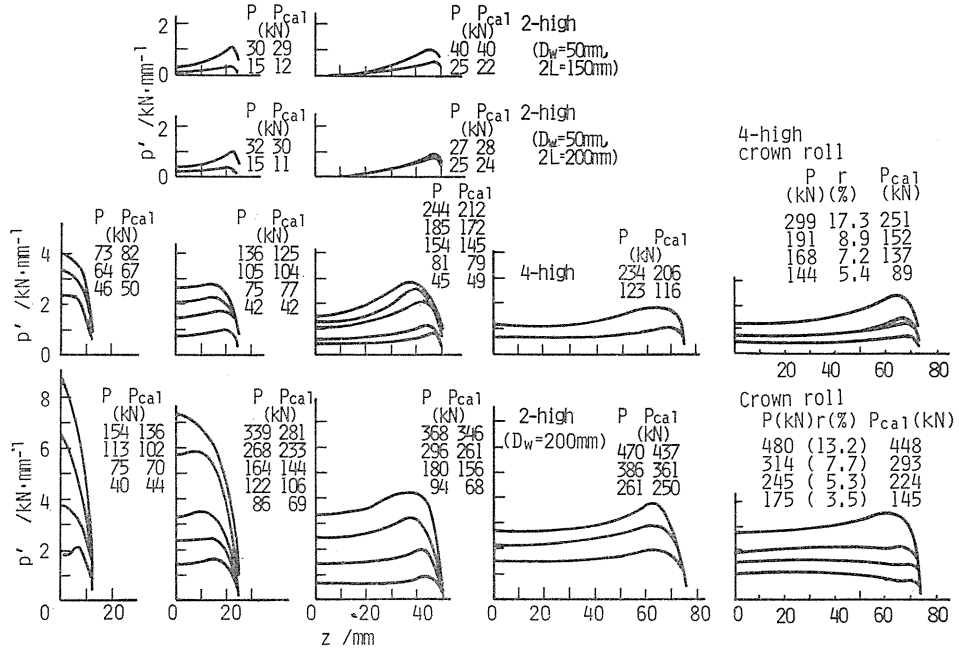

Fig. 1. 12 Distribution of rolling force per unit width across the strip width.

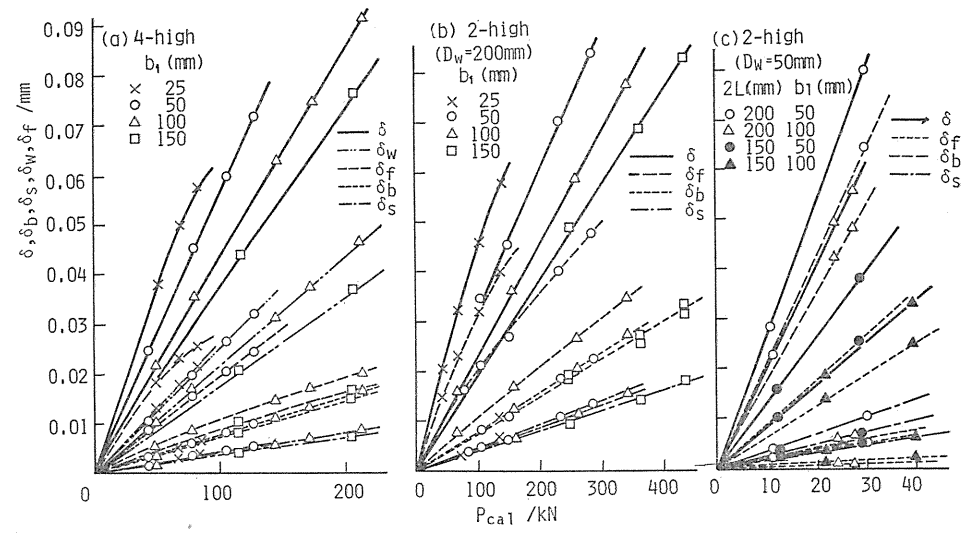

Fig. 1. 13 Relationship between calculated rolling force and each component of the roll deformation at centre (z=0).

small to the other components.

In case of 2-high (D_W=200mm) (Fig. b)), δ_b, δ_s and δ_f change with rolling force in similar way as 4-high.

In case of 2-high (D_W=50mm) (Fig. (c)), δ_b is extremely large and δ is not influenced very much by δ_s and δ_f, because the stiffness of roll is small.

Effect of strip width on each component of roll deformation at the centre under the condition of same reduction is shown in Fig. 1. 14. As rolling force is almost proportional to strip width, δ_b and δ_s are in proportion to strip width in all cases. But the distribution of rolling force varies with strip width, therefore δ_f also varies with strip width.

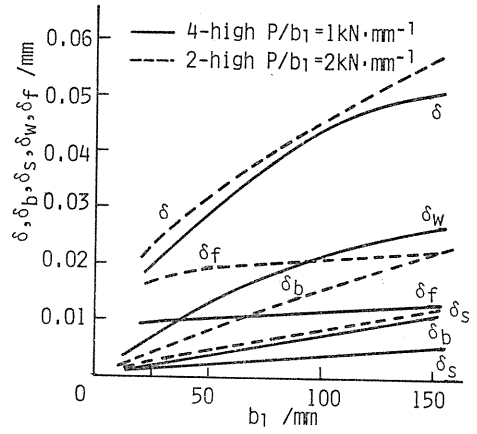

Fig. 1. 14 Effect of the strip width b_1 on each component of the roll deformation at the centre (Rolling force per unit width is constant for each of 4-high and 2-high.)

1. 5. Discussion

1. 5. 1. Comparison of calculated results with experimental ones

a) Rolling force

Calculated rolling force P_{cal} is shown in Fig. 1. 12 together with measured one P. In case of 2-high (D_W=50mm), the both rolling forces almost coincide with each other. Besides, the calculated result of total deflection δ agrees well with experimental result (see Fig. 1. 11(a)), so the present analysis is proper when roll is considered as a simple beam like this case. Fig. 1. 15 shows the comparison of the total rolling force between the measured value and the calculated one.

In case of 2-high (Fig. (a)), P_{cal} is 1 %~23% smaller than P and the calculated result of δ doesn't always agree with experimental one. The reason is considered that roll is restrained from inclining at the bearing box which is supported between the columns of mill housing. Then, the deflection caused by the moment of restriction at the supporting point is introduced in the analysis as follows.

When bending moment M is applied to both edges of roll, the deflection of roll at z_i from the centre by M, $(\delta_m)_i$, is expressed as follows.

$$(\delta_m)_i = a_i' \cdot M \tag{1.61}$$

After this equation is added to Eq. (1. 57) or Eq. (1. 58), $p_j'(j=1\sim n)$ and M can be calculated by the same way.

The broken line in Fig. 1. 11(b) and (f) show the results obtained by this calculation and δ_m is the deflection of roll by M. P_{cal} is a little larger than P, but the distribution of δ agrees well with the experimental result. P_{cal} calculated by this method is also plotted in Fig. 1. 15(a). It is found that good results are obtained by taking the restriction of moment into consideration in case of 2-high.

In case of 4-high (Fig. 1. 15(b)), P_{cal} is larger than P for the condition of small rolling force but its tendency is reversed when rolling force is large.

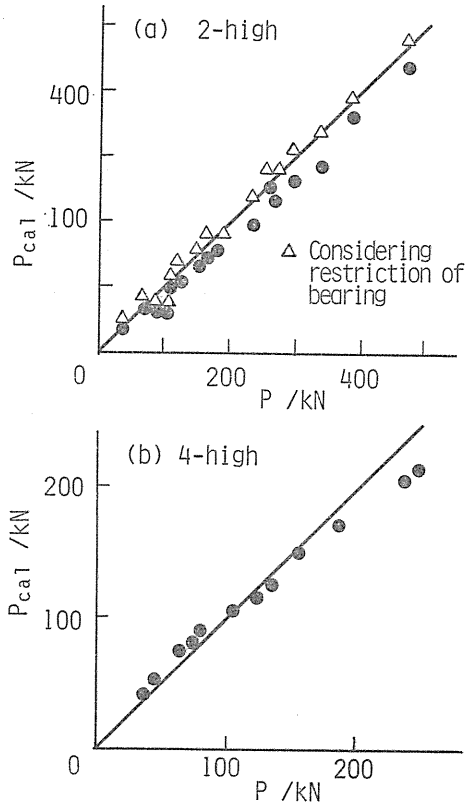

Fig. 1. 15 Comparison of the total rolling force between the experimental value P and the calculated one P_{cal}.

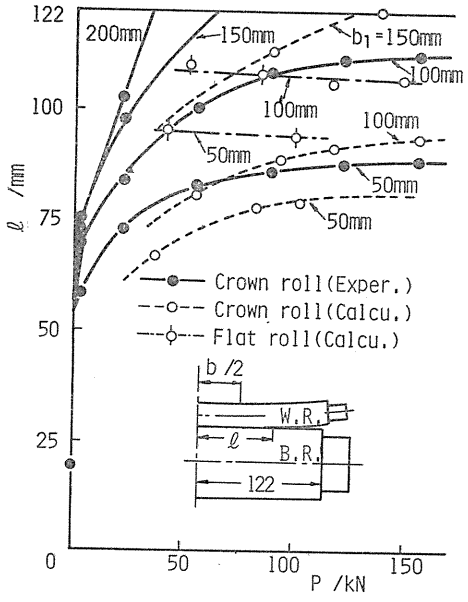

Fig. 1. 16 Contact width l between work roll and backup roll.

Besides, good results are not always obtained when the restriction of moment is considered.

In case of 4-high, there are two problems in this analysis. One is that the elastic constant c is assumed to be constant even if the contact force between work roll and backup roll q' changes. The other is that the contact force q' is zero near the edge of roll barrel and becomes positive at the edge (see Fig. 1. 11(c), (d), (e)).

b) Contact width between backup roll and work roll

Contact width between backup roll and work roll l is obtained by measuring the shielded width of light which is sent from entry side, when strip is statically loaded.

Calculated contact width is shown in Fig. 1. 16 together with the measured results. The calculated result is smaller than the measured one in all conditions but both results agree qualitatively. There are some reasons in the difference of both results. One is that the analysis is not perfect. The other is that the calculated result means the width on which the contact force q' is applied or not zero, while it is expected that both rolls contact each other without any contact

force. There are some problems in the present analysis as justmentioned but they don't affect the distribution of p' and that of δ, δ_b, δ_s and δ_f in the contact region with strip, therefore this analysis is effective in order to clear the influence of roll deflection on the distributions of rolling force and strip thickness.

1. 5. 2. Distribution of rolling pressure along the arc of contact

Rolling pressure generally distributes convexly along the rolling direction. In this analysis, it is assumed as uniform along the arc of contact, so an effect of this assumption is discussed by comparing with a result calculated by assuming its distribution as an ellipse. The result shows that the distribution of rolling force doesn't change and the total rolling force is only 2% larger than the case of uniform distribution.

1. 5. 3. Effect of roll crown

In case of 2-high, the non-uniformity of thickness across the strip width decreases by use of crown rolls and the distribution of rolling force also becomes uniform (see Fig. 1. 12) and its effect becomes notable when wide strip is rolled.

In case of 4-high, the strip crown is improved by use of crown roll because of the decrease in the deflection of work roll. On the other hand, there is little effect of crown roll on the distribution of rolling force.

1. 6. Conclusions

The elastic deformation of rolls by rolling force, which is divided into three components (Deflection of backup roll, deflection of work roll and flattening of work roll surface), is analyzed. And the analysis to obtain the distribution of rolling force per unit width from the measured contour of deformed roll is presented. Not only the distribution of rolling force but also the contact force between backup roll and work roll and each component of roll deformation can be obtained. The influence of rolling conditions on them is investigated and the results may be summarized as follows.

(1) The rolling force per unit width isn't uniform across the strip width and the pattern of its distribution changes with rolling condition. It is convex for narrow strip and concave for wide strip. The contact force between work roll and backup roll in case of 4-high becomes maximum at the centre of roll barrel and its distribution looks like a parabola.

(2) When strip is wide, the flattening of work roll surface gradually increases from the centre towards the edge and attains to the maximum near the edge, while the deflection decreases monotonically from the centre to the edge. As a result, the strip thickness is uniform near the centre of width independently of rolling force.

(3) The non-uniformity of thickness across the strip width in case of 4-high is worse than that in case of 2-high because of the existence of deflection of work roll.

(4) The distribution of rolling force becomes uniform when crown roll is used in case of 2-high but there is littel effect of crown roll on that in case of 4-high.

(5) The present analysis is effective in order to clear the influence of roll deflection on the distribution of rolling force and strip thickness.

Part 2. Measurement of the Distritbuion of Rolling Pressure

YASUHISA TOZAWA, TAKASHI ISHIKAWA, TAKASHI KATO,
MASAO NAKAMURA, KENJI INOUE and NORIAKI KATO

2. 1. Introduction

In order to measure the distribution of rolling pressure during rolling directly, the method, so-called the pin method, in which the pressure pin is inserted in a roll and applied load is detected by load-sensor, has been adopted. Siebel and Lueg measured the pressure distribution by the pin method first[22]. There are many papers about the rolling pressure measured by the pin method[23~26]. Matsuura and Motomura measured pressure distribution for many kinds of rolling conditions and classified the distribution into three kinds of pattern[27~29]. But in their experiments, a roll with only one or a few pressure-sensors is used and pressure distribution across the strip width is measured by rolling many strip specimens at different relative position in roll barrel to the sensor. In fact, it is very difficult to keep same condition for each rolling, and moreover it costs us much labor and time. On the other hand, measurement by using multi-channelled sensors was carried out by Vater[30] which is the only one experiment up to now, but it was the problem that the amount of scatter in measured pressure and hole for inserting sensors into roll was large.

In order to measure rolling pressure distribution across the width of strip using multi-channelled pressure-sensor, a new system is designed and developed. In the system, a micro-computer is used as a main processor and the flexible software which involves a continuous sampling method and a data processing method is applied. The most suitable conditions of pin and roll are investigated and then the pressure distribution are measured for various rolling conditions using the developed system.

2. 2. Development of multi-channelled measuring system

Fig. 2. 1 shows the block diagram of the system developed newly. A micro-computer with i 8080 CPU and 48 K byte memories is used as a central processor. Analogue data from multi-channelled sensors are sampled simultaneously by a sample-holder through multi-channelled low noise DC-amplifiers and immediately converted to digital data by A/D converter, then stored in a floppy disk sheet. The amplifiers, sample-holder, A/D converter and interfaces are made by the authors themselves. Other peripheral instruments and their functions are as follows; a keyboard for input of initial data, a character- and a graphic-display for monitor at real time, an X-Y recorder and a printer for output of sampled data. These instruments are connected to the computer by a common bus line. The system is controlled by the flexible software programmed by Assembly languages. Also the system is used for the development of software or the calculation of sampled data. The general view of this system is shown in Fig. 2. 2.

During rolling the pressures at thirteen points in the half-width of strip are sampled simultaneously and after rolling sampled data are output as a diagram directly by an X-Y recorder. Therefore the obtained results can be judged and evaluated immediately in the place.

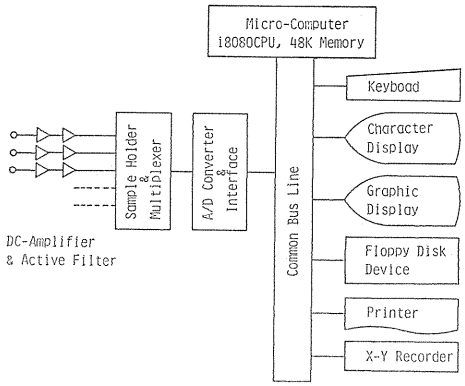

Fig. 2. 1 Block diagram of the meausuring system.

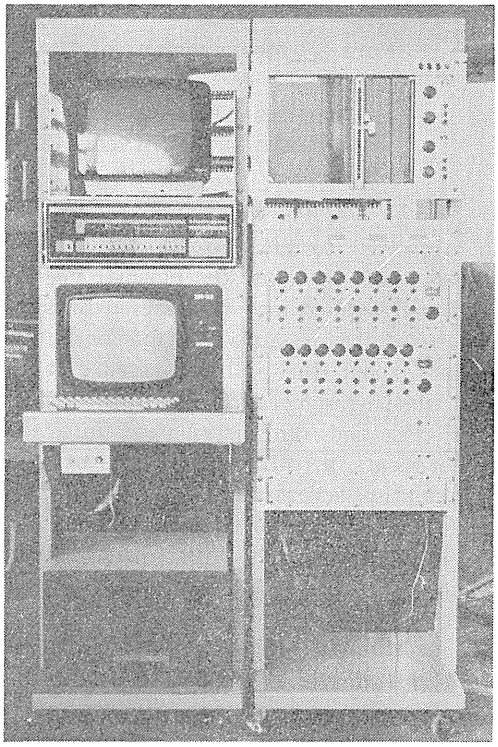

Fig. 2. 2 General view of the measuring system.

The characteristics of this system are as follows.

(1) Man-power and personal error are reduced as far as possible in sampling data.

(2) The sampled data can be monitored in real time and the obtained results can be judged immediately in the place.

(3) The sampled data can be stored in the floppy disk sheet so it is easy to analyze the data afterward.

2. 3. Construction of roll and pressure sensor

Rolling mill used in the experiment is 2-high mill having flat rolls 210 mm dia. of barrel length 250 mm. The segment, in which thirteen pins of 1 mm diameter and load cells are inserted at interval of 6 mm, is bolted on the lower roll as shown in Fig. 2. 3. In the design of this roll, avoiding large decrease in the stiffness of roll by the pin hole and the groove for lead is minded, which is one of the important problems in the pin method. Two strain gauges of which gauge length is 0. 3 mm are cemented on the load cell and the calibration of load cell is carried out with INSTRON testing machine. The projecting height of pin is adjusted by changing the length of the adjusting rod.

There is no difference between the stiffness of a solid roll and that of the roll for measuring the pressure (Fig. 2. 4). Further discussion about the stiffness of roll will be presented later.

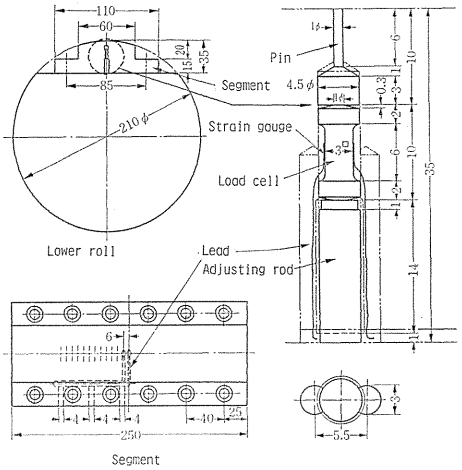

Fig. 2. 3 Details and assembly of the roll for measuring the pressure.

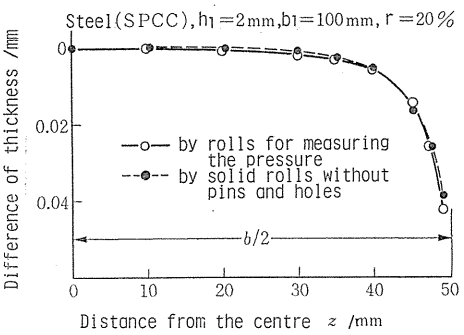

Fig. 2. 4 Distribution of thickness across the width of rolled strip.

2. 4. Investigation about measuring condition

2. 4. 1. Influence of projecting height of pin on the distribution of rolling pressure

The projecting height of pin (Ψ) is defined as the depth of an impression on the surface of rolled strip. Fig. 2. 5 shows the distribution of rolling psessure along the arc of contact at the centre of strip width. The pressure detected by a pin increases with increasing in the projecting height and the peening peak occurs when the projecting height is large. But the distributions for small or negative projecting height are similar to each other. Therefore, the proper condition of the projecting height seems to be zero or a little negative from the point of the distribution pattern of detected pressure.

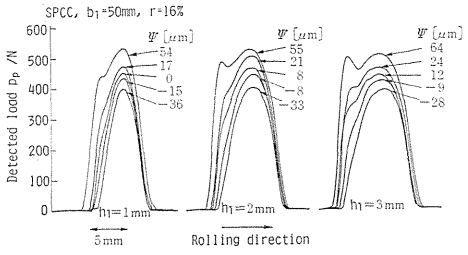

Fig. 2. 5 Influence of strip thickness (h_1) and projecting height of pin (Ψ) on the distribution of rolling pressure.

2. 4. 2. Influence of projecting height of pin on detected load

Fig. 2. 6 shows the variation of the load detected by a pin with compressive load when a specimen ($10\times20\times2$mm) is compressed on the segment. The detected load changes widely by the projecting height even if same load is applied. Fig. 2. 7 is the relation between the projecting height of pin and the detected load for each compressive load in compression test. Variation of the detected load with the

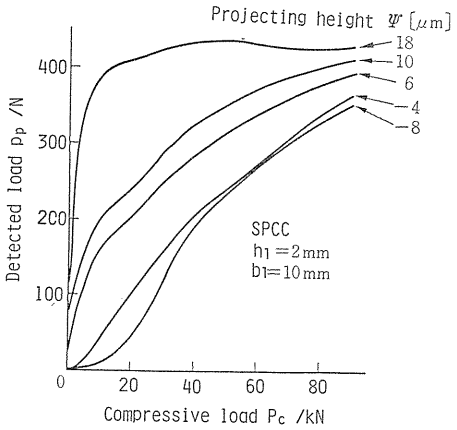

Fig. 2. 6 Influence of the projecting height of pin (Ψ) on the load detected by a pin (p_p) (in compression test).

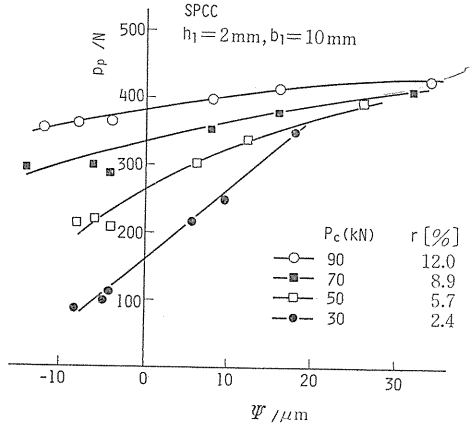

Fig. 2. 7 Relation between projecting height of pin (Ψ) and the detected load (p_p) (in compression test).

projecting height becomes remarkable with the decrease in compressive load (or reduction in thickness), so the projecting height of each pin must be adjusted accurately to a certain height for low reduction in case that the pressure is measured by multi-channelled pin.

2. 4. 3. Relative stiffness of pin and roll

The projecting height of pin which is adjusted to zero initially, decreases with increase in reduction or rolling force when narrow strip is rolled and this tendency becomes weak with the increase in strip width, see Fig. 2. 8.

It is expected to be a reason that the deformation of pin is determined by the pressure applied to a top of pin but roll, which is continuous body, is deformed by the pressure around the pin. In order to confirm this, flattening of roll surface by uniform rolling force is calculated from the equation which is presented in Part

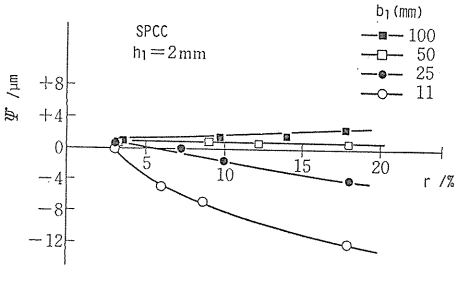

Fig. 2. 8 Relation between projecting height of pin (Ψ) and rolling reduction (r) for each strip width (b_1).

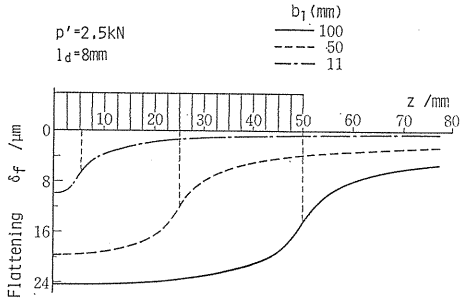

Fig. 2. 9 Effect of strip width on flattening of roll surface (Calculated from the uniform distribution of rolling force per unit width p').

1 and the result is shown in Fig. 2. 9. The deformation at the centre of strip width increases with the increase in strip width, in spite of the rolling force acting at the point is unchanged. On the other hand, the deformation of pin is constant and independent of strip width. Therefore the projecting height during rolling decreases with the decrease in strip width, as shown in Fig. 2. 8. It is found from Fig. 2. 8 that the relative stiffness of pin is almost same as that of roll when the strip width is 50 mm and 100 mm, so the adjusting rod which is made of steel bar (SGD) of 4.5 mm dia. used in this case is appropriate. The stiffness of pin, however, may be relatively low for narrow strip.

2. 4. 4. Clearance between pin and pin hole

Diameter of pin used in this measuring device is 0.965 ± 0.005 mm and clearance is about 0.05 mm. When pressure is calculated from the detected load, the calculated pressure should change with the cross-sectional area used in the calculation. Fig. 2. 10 shows the relation between the calculated pressure and the ratio of cross-sectional area of pin A_p to that of pin hole A_h when a given load is applied. It is considered that the exact pressure is obtained when $A_h = A_p$. So, it is found that the effective cross-sectional area for calculation of pressure is 0.75 mm^2 (corresponds to that of diameter 0.977 mm) by extrapolating the data to $A_h = A_p$ in Fig. 2. 10.

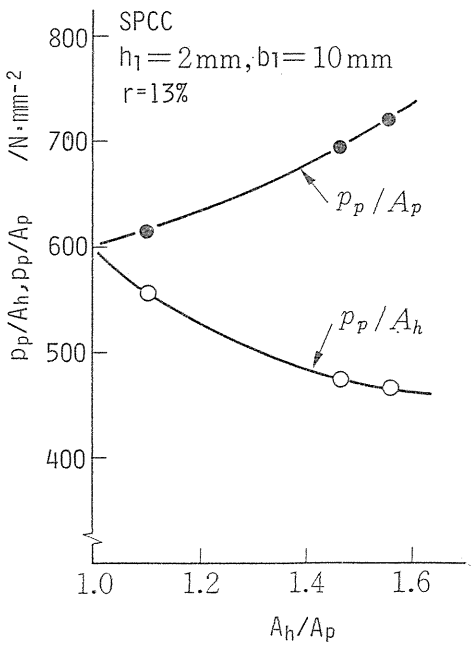

Fig. 2. 10 Correction of the cross-sectional area of pin to calculate the pressure. A_p, A_h: cross-sectional area of pin and hole respectively.

2. 4. 5. Examination of the validity of the measuring method

a) Rolling force

Rolling force obtained by integrating the measured pressure (cf. Fig. 2. 15) over the contact area agrees well with that measured by load cell which is placed between the screw and the roll chock for various rolling conditions as shown in Fig. 2. 11, so the measuring method and the adopted condition are appropriate.

b) Comparison with the calculated results

Fig. 2. 12 shows the distribution of rolling force and each component of roll deformation, which is calculated from the equations presented in Part 1, when a strip is rolled by the roll for measuring the pressure. Each component of roll deformation is rewritten as follows.

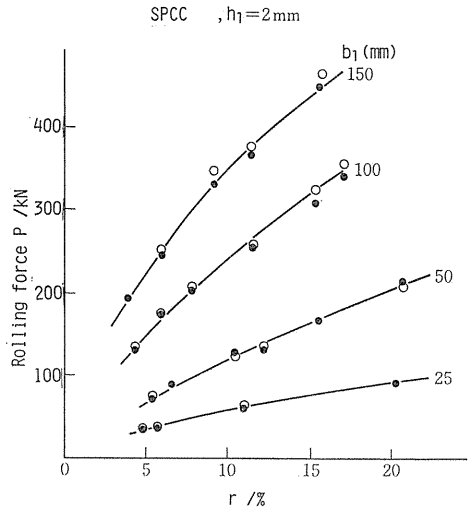

Fig. 2. 11 Comparison of rolling force calculated from the measured pressure distribution (-○-) with that obtained by load cell (-◎-).

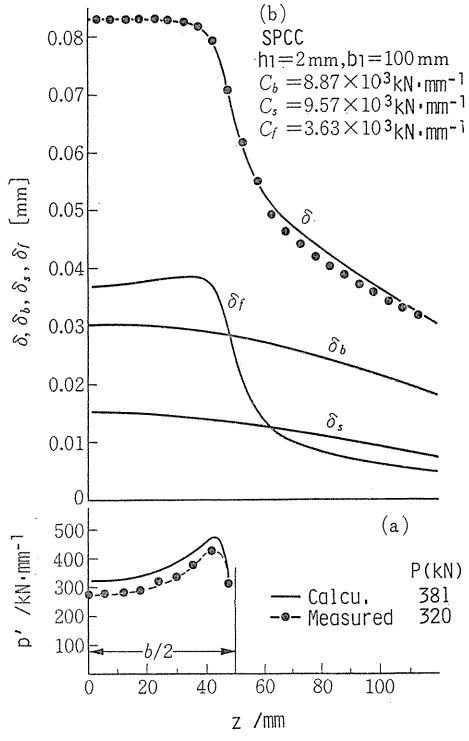

Fig. 2. 12 (a) Comparison of the distributed rolling force per unit width in the transverse direction obtained by measurement with that calculated analytically from the deformed roll profile.
(b) Components of the deformation of roll obtained analytically.

$$(\delta_b)_i=\frac{1}{C_b}\sum_{j=1}^{n} p_j'\cdot w\cdot F_b,\quad C_b=\frac{6E_RI_R}{L^3} \tag{2.1}$$

$$(\delta_s)_i=\frac{1}{C_s}\sum_{j=1}^{n} p_j'\cdot w\cdot F_s,\quad C_s=\frac{3A_RG_R}{4L} \tag{2.2}$$

$$(\delta_f)_i=\frac{1}{C_f}\sum_{j=1}^{n} p_j\cdot w\cdot F_s,\quad C_f=\frac{\pi E_R w}{1-\nu_R} \tag{2.3}$$

where E_R, G_R, ν_R, A_R and I_R are Young's modulus, shear modulus, Poisson's ratio, cross-sectional area and moment of inertia of area of roll respectively and w is finite width to which rolling force per unit width p_j' is applied and F_b, F_s and F_f are non-dimensional quantities. The distribution pattern of rolling force p' is

similar to that obtained by the pin method but total rolling force calculated is larger than measured result. Then, the calculation is carried out under the other conditions that the stiffness factor for bending C_b and that for flattening C_f are changed independently. The results of total rolling force agree well with the measured one when either C_b or C_f is lowered (Fig. 2. 13), so it is found that the stiffness of roll for measuring the pressure is lower than a solid roll but its effect on the profile of rolled strip is very small (see Fig. 2. 4).

2. 6. Results

Mild steel (SPCC) of thickness 2 mm and 1 mm, duralumin (A2017) aged and annealed and aluminium (A1050) annealed of thickness 2 mm of which stress-strain cruve are shown in Fig. 2. 14 are used. Rolling speed is 0. 4 rpm.

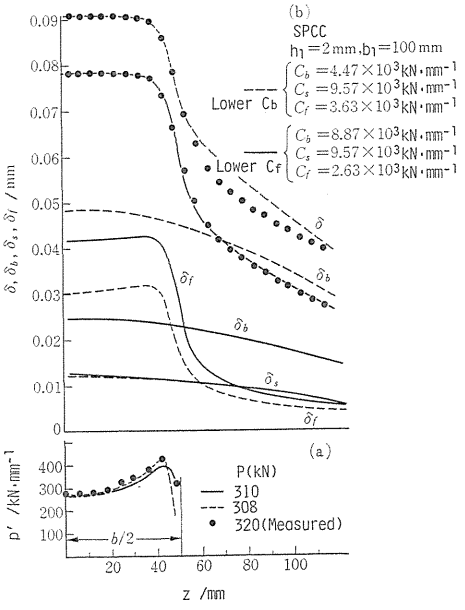

Fig. 2. 13 Influence of roll stiffness on the calculated results.
(a) Distribution of rolling force per unit width (p'),
(b) Deformation of roll.

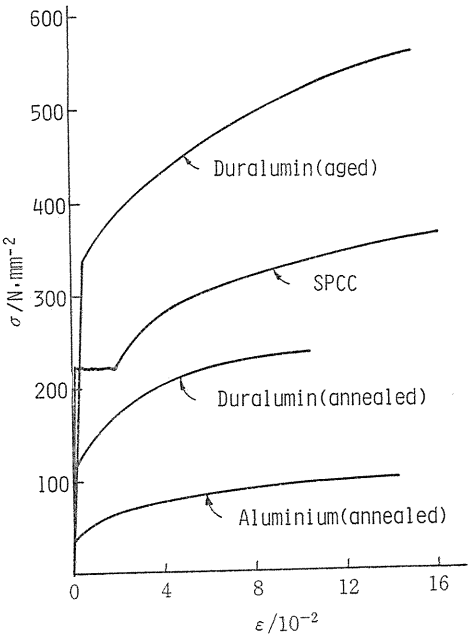

Fig. 2. 14 Stress-strain curve in tension of the material used.

2. 6. 1. Influence of strip width and reduction

The distributions of rolling pressure for two kinds of strip width and reduction are shown in Fig. 2. 15. The location of maximum pressure in the arc of contact, which is considered as a non-slip point, is near the centre a little inclined towards the exit of roll gap and the same across the strip width. Fig. 2. 16 shows the distribution of rolling force per unit width, which is obtained by integrating the rolling pressure along the each arc of contact. Peak of rolling force exists

near the edge of strip except for the narrow strip. The peak moves towards the centre of strip width with the increase of reduction. These results are almost same as that obtained from the contour of deformed roll shown in Fig. 1. 12.

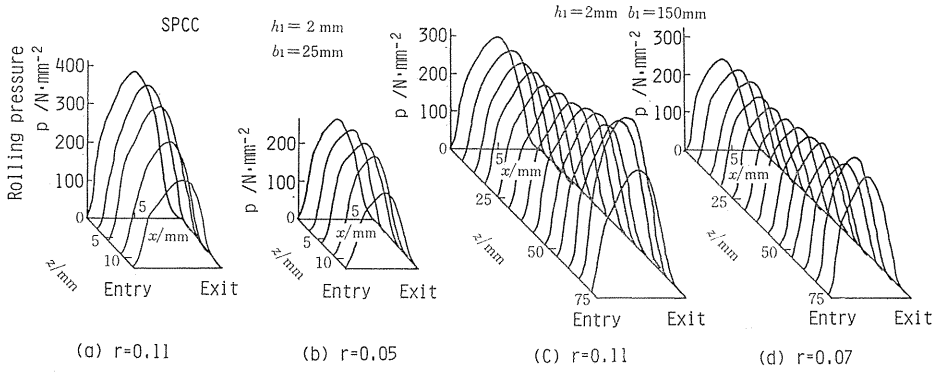

Fig. 2. 15 Influence of reduction r on the distribution of rolling pressure p for mild steel varied with strip width b_1.

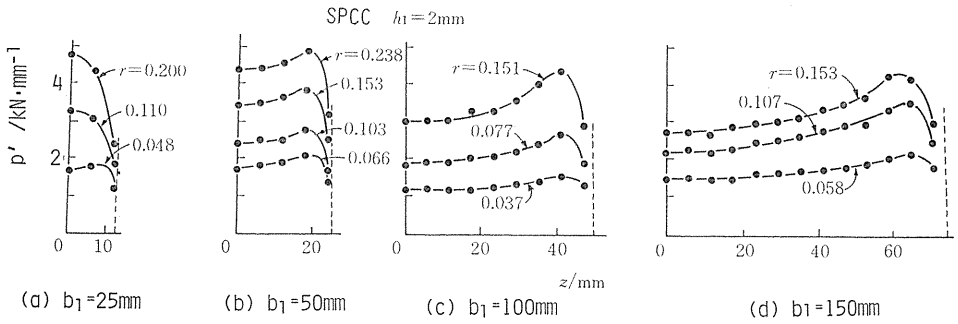

Fig. 2. 16 Influence of reduction r on the distribution of rolling force per unit width p' for mild steel varied with strip width b_1.

2. 6. 2. Influence of yield stress of strip

The distribution pattern of rolling force changes with the yield stress of strip and the peaks of rolling force near the edges are made sharp by the increase of yield stress of strip to be rolled when strips are rolled under a given reduction (Fig. 2. 17). On the other hand, when strips are rolled under a given rolling force, there is a large difference in the distribution of rolling pressure as shown in Fig. 2. 18, because of difference in the reduction or the length of contact arc. In this case, the peaks of rolling force move close to the edges as the yield stress increases (Fig. 2. 19).

2. 6. 3 Influence of front- and/or back-tension

Fig. 2. 20 shows the distribution of rolling pressure when front- and / or back-tension is applied. It is found that the distribution along the arc of contact changes with tension in the same manner as the result obtained from the theory of rolling (Fig. 2. 21). Fig. 2. 22 shows the influence of tension on the distribution of

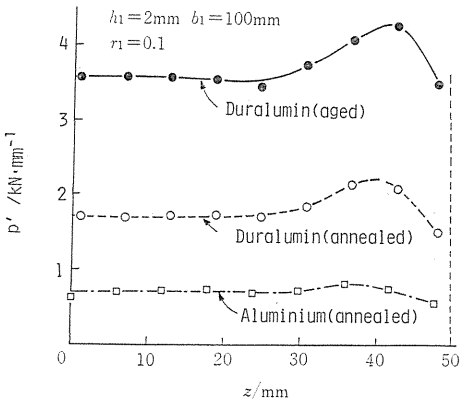

Fig. 2. 17 Influence of yield stress of material on the distribution of rolling force per unit width p' across the strip width.

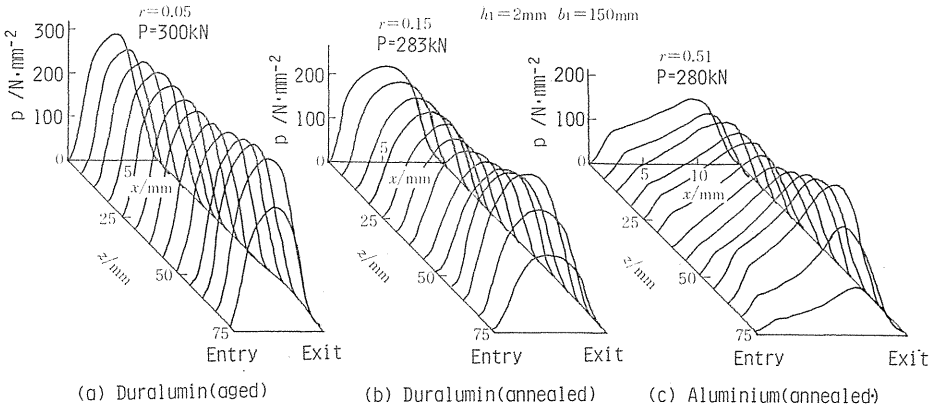

Fig. 2. 18 Influence of yield stress of material on the distribution of rolling pressure p under the condition of a given rolling force P.

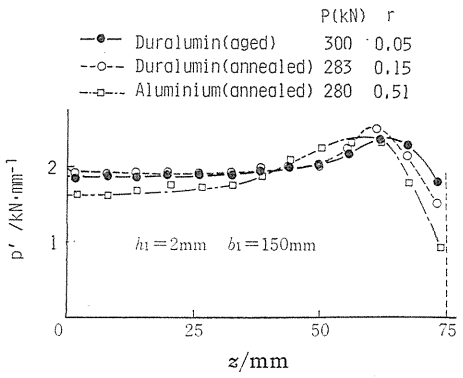

Fig. 2. 19 Influence of yield stress of material on the distribution of rolling force per unit width p' under the condition of a given rolling force P.

rolling force. The rolling force per unit width decreases largely at the centre of strip when front-tension is applied, while the peak value of rolling force near the edge decreases largely when back-tension is applied. On the other hand, the rolling force at the edge of strip hardly changes with tension.

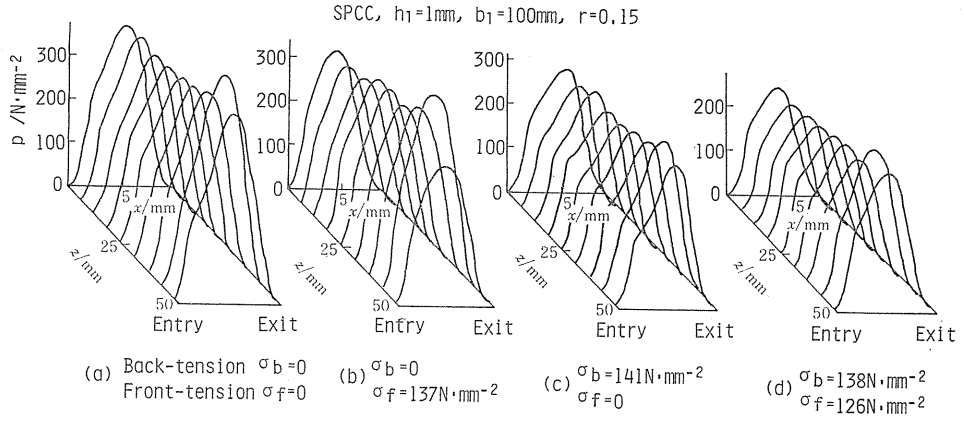

Fig. 2. 20 Influence of front-tension σ_f and back-tension σ_b on the distribution of rolling pressure p for mild steel strip.

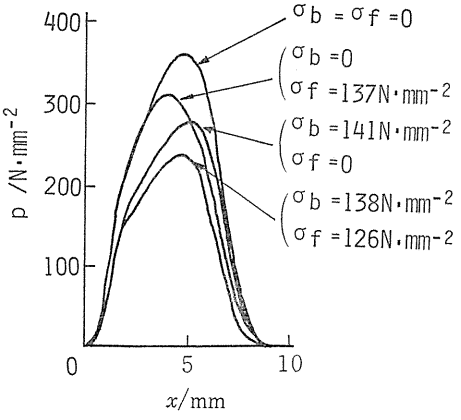

Fig. 2. 21 The distribution of rolling pressure p along the arc of contact at the centre of width for mild steel strip.

2. 6. 4. Comparison with other experimental results

There are many papers about the distribution of rolling pressure measured by the pin method[22~26]. But almost all of them are limited for narrow strip, and show that the peak of rolling force exists at the centre of strip width like as Fig. 2. 16(a). There were few researches in which the reasonable results were obtained for wide strip. Matsuura et al. classified the distribution into three kinds of pattern (convex, flat and concave) and presented the classification table[27~29]. Results measured in the present paper almost agree with not only theirs but the results determined from the measured contour of deformed roll (see Part 1) and also that calculated by using the three-dimensional analysis[32].

2. 7. Conclusions

The multi-channelled measuring system is developed newly to measure the distribution of rolling pressure by the pin method first, and the most suitable

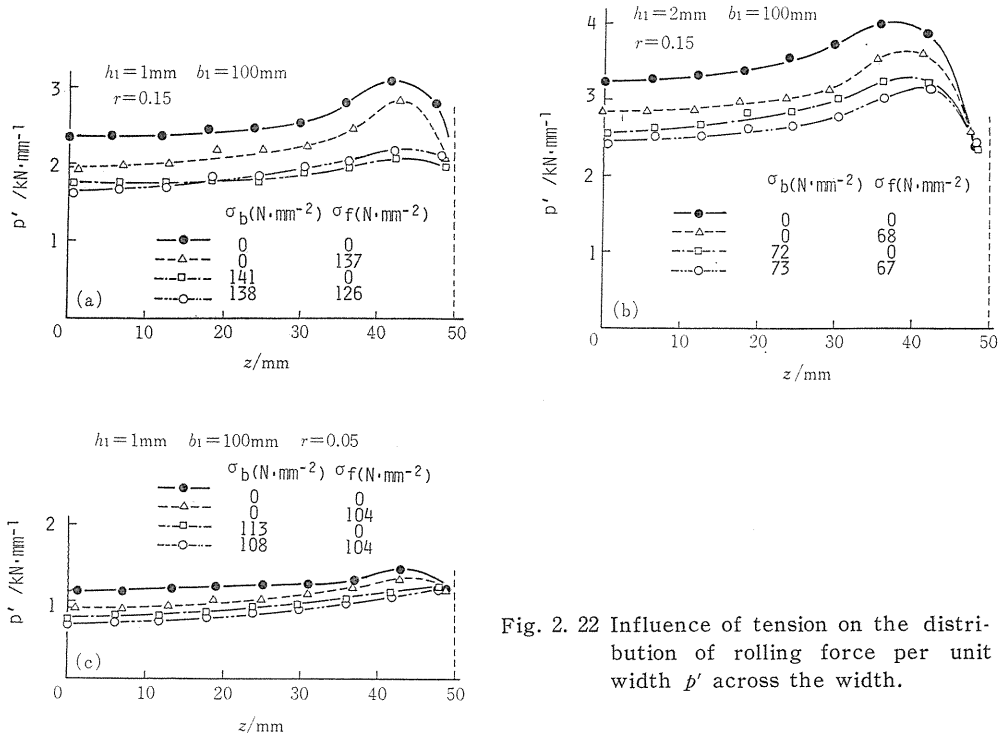

Fig. 2. 22 Influence of tension on the distribution of rolling force per unit width p' across the width.

conditons of pin and roll are investigated and then distribuitons of rolling pressure are measured for various rolling conditions. The results may be summarized as follows.

(1) Using the developed system, man-power and personal error are reduced and the obtained results can be judged immediately in the place.

(2) The most suitable projecting height of pin is zero and it is necessary that the stiffness of pin is equal to that of roll.

(3) The reliability of the results obtained from this system and the condition adopted is very high.

(4) The location of maximum pressure in the arc of contact is the same across the strip width even if tension is applied.

(5) The distribution pattern of rolling force per unit width is always concave when wide strip is rolled.

(6) Tension acted on the strip is effective to decrease the total rolling force, whereas it doesn't almost change the rolling force at the edge.

Part 3. Distribution of Stress at the Upper Stream Side of Roll Gap

YASUHISA TOZAWA, TAKASHI ISHIKAWA, MASAO NAKAMURA,
TAKASHI KATO and YASUNARI ITO

3. 1. Introduction

Though the other stresses in the region of roll gap than the rolling pressure are not measured, they arise stresses at the outside of roll gap because of the continuity of strip. Therefore if the stress distribution at the outside of roll gap would be measured, the stresses at the entry of roll gap have been determined as the boundary condition. The stress distribution at the upper stream side of roll gap has been measured for a narrow strip only[31].

In part 3, strains at the upper stream side of roll gap during rolling are measured under the several kinds of rolling condition and the stresses are calculated from the measured values. On the other hand, the stresses at there are calculated by FEM from the assumed stresses at the entry of roll gap and by comparing both calculated results the stresses at the entry of roll gap are estimated.

3. 2. Experimental procedure

3. 2. 1. Rolling mill and specimen

Rolling mill used in the experiment is 2-high single stand mill having flat rolls 200 mm dia. of barrel length 250 mm. Mild steel (SPCC) strip of 2 mm thickness and 150 mm and 50 mm width is used as a specimen.

3. 2. 2. Rolling condition and measuring method

Strip of 900 mm length and rolls are degreased with acetone prior to each experiment. Rolling speed is 0.4 rpm. In order to measure the strains at the ingoing strip, strain gauges, 2-axial rosette type, are stuck on both surfaces of a strip to be rolled. And another gauge of which shielding film is removed before rolling is also stuck on one surface as shown in Fig. 3. 1, in order to determine a moment at which the gauges reach the entry of roll gap from the signal which is produced when this gauge contacts with roll. Position of the gauges during rolling is counted backward from the movement of strip measured by a distance meter. By using the multi-channelled measuring system introduced in Part 2, multi-channelled strain is sampled simultaneously at every interval of a strip movement of 0.4 mm. The sampled data are output as a diagram directly by an X-Y recorder and stored in a floppy disk sheet and then it is transmitted to a large compuer in

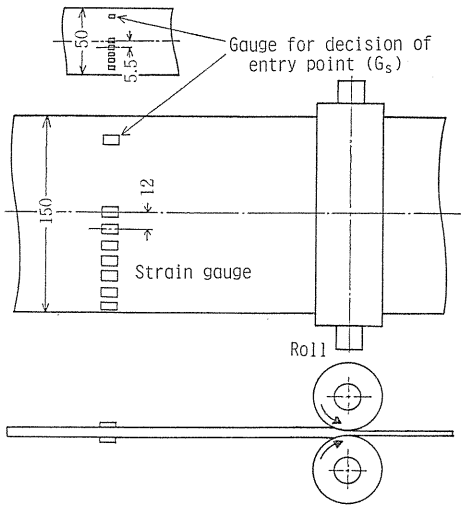

Fig. 3. 1 The position of strain gauges stuck on strip.

order to calculate stresses and draw the results as a distribution map.

3. 3. Results

3. 3. 1. Examples of the results

Distributions of longitudinal strain ε_x and transverse strain ε_z along rolling direction at each position drawn by an X-Y recorder is shown in Fig. 3. 2. It is found that strain occurs far away from the entry of roll gap and the distributions differ with the position across the strip width. Fig. 3. 3 shows the distributions of longitudinal stress σ_x and transverse stress σ_z calculated from the measured strains.

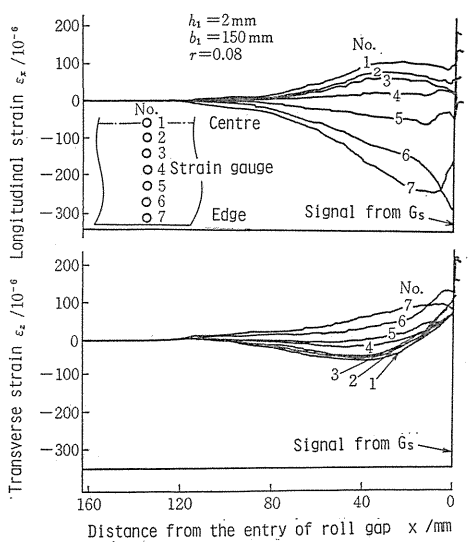

Fig. 3. 2 Strain of each place (No. 1 ~ No. 7) at the distance x from the entry of roll gap.

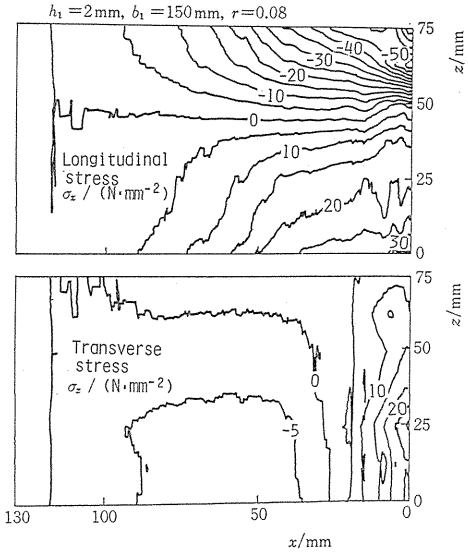

Fig. 3. 3 The distributions of longitudinal stress σ_x and transverse stress σ_z at the upper stream side of roll gap.

Distributions of σ_x and σ_z across the strip width at the entry of roll gap (x= 0) and at the upper stream side (x=70.2 mm) shown in Fig. 3. 4. σ_x is tension at the centre of strip width and compression near the edge and their values increase as x decreases though there is a peak of compressive stress near the edge at the entry of roll gap. On the other hand σ_z is zero at the edge of strip because of the free end and it changes from compression to tension as x decreases.

Fig. 3. 5 shows the distributions of stresses for narrow strip (b_1=50 mm). Stresses occur at nearer region to the entry of roll gap than the case of wide strip and the distribution pattern is different from the case of wide strip (Fig. 3. 3).

3. 3. 2. Influence of reduction and strip width

Distributions of σ_x and σ_z at the entry of roll gap are shown in Fig. 3. 6 and

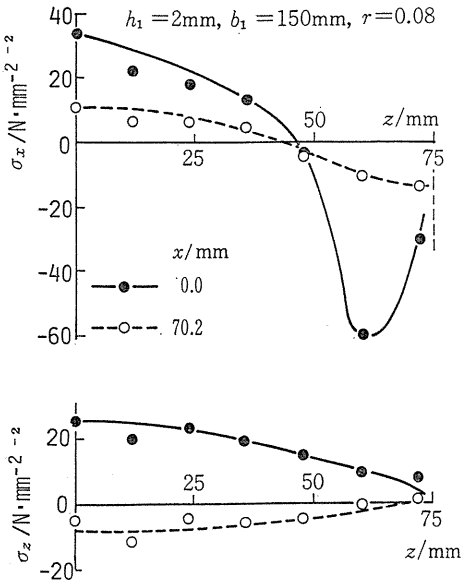

Fig. 3. 4 The distributions of longitudinal σ_x and transverse stress σ_z at the entry (x=0) and at the upper stream side (x=70.2 mm) of roll gap.

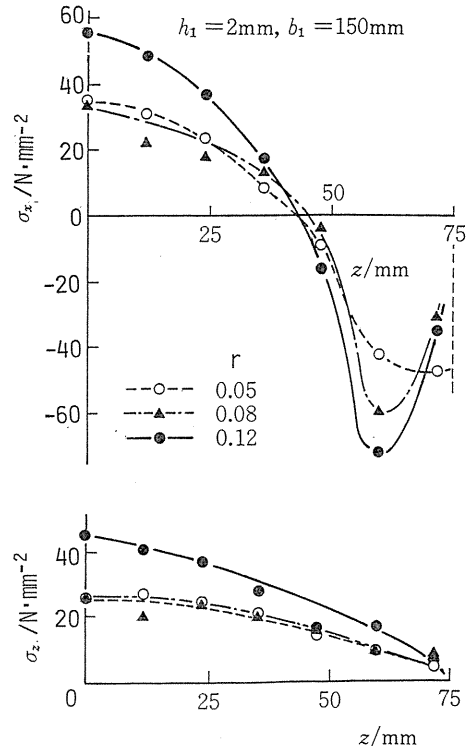

Fig. 3. 6 The distributions of stresses at the entry of roll gap for wide strip.

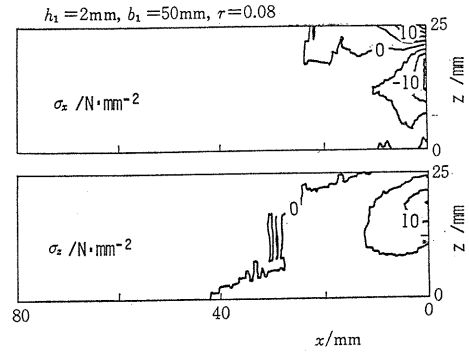

Fig. 3. 5 The distributions of stresses at the upper stream side of roll gap.

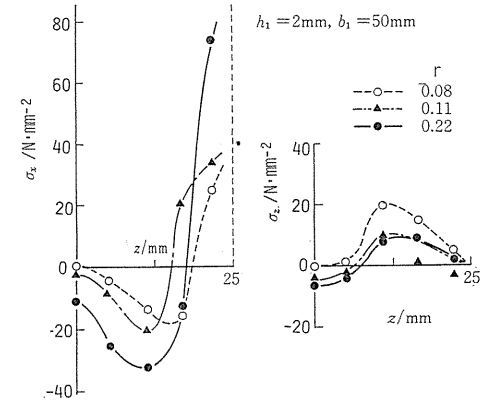

Fig. 3. 7 The distributions of stresses at the entry of roll gap for narrow strip.

Fig. 3. 7. In case of wide strip (Fig. 3. 6), the compressive peak of longitudinal stress near the edge becomes sharp as reduction increases while distribution of transverse stress changes monotonously. On the other hand, in case of narrow strip (Fig. 3. 7), tensile value of longitudinal stress at the edge of strip width increases with increase of reduction while the change in the distribution of transverse stress is small.

The position of the appearance of the stresses (x_c) goes away from the entry of roll gap with increase of reduction and especially with the increase of strip width (Fig. 3. 8).

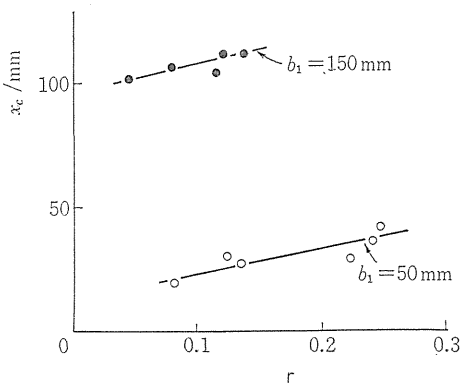

Fig. 3. 8 The position of the appearance of strain x_c.

3. 3. 3. Influence of tension

There is almost no effect of front-tension on the distribution of stresses at the upper stream side of roll gap as shown in Fig. 3. 9. The transverse stress

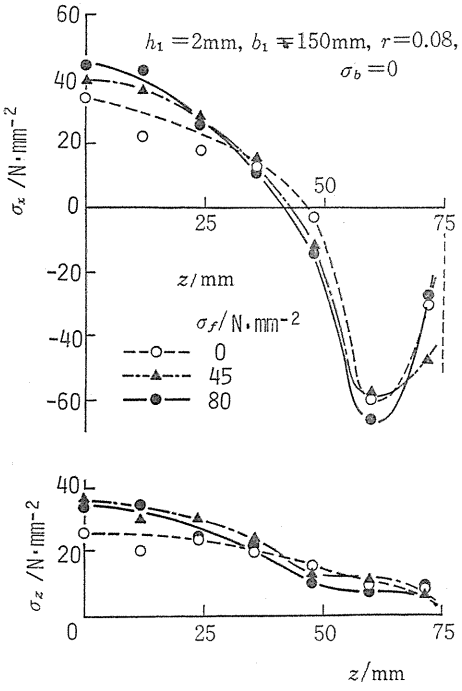

Fig. 3. 9 The distributions of stresses at entry of roll gap.

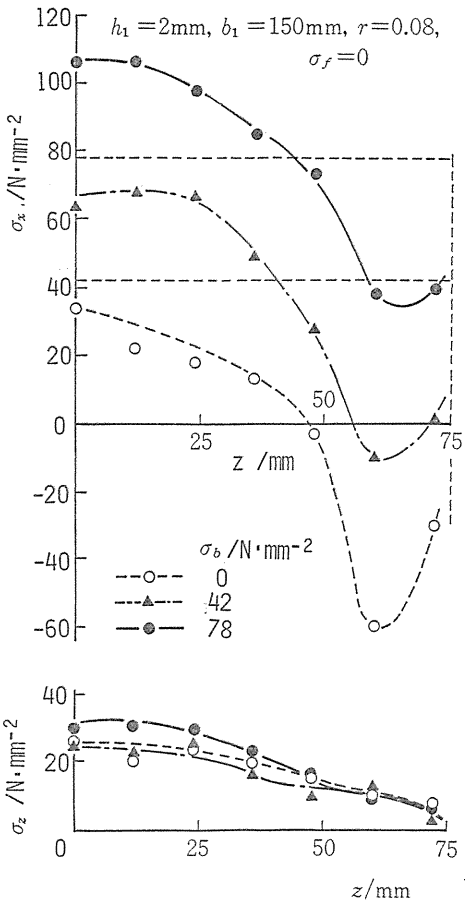

Fig. 3. 10 The distributions of stresses at the entry of roll gap.

is not affected by back-tension but the longitudinal stress is shifted to tensile side and the difference between the maximum stress and the minimum stress decreases with the increase of back-tension (Fig. 3. 10).

3. 4. Discussion

The distributions of the longitudinal stress at the entry of roll gap across the strip width obtained experimentally agree with the results of the three-dimensional analysis for the region in roll gap[32], and it is supposed that the appearance of the stresses at the upper stream side of roll gap is due to the stresses at the entry of roll gap. So the distribution of stresses at the upper stream side is calculated by Finite Element Method (FEM) from the stresses at the entry of roll gap.

Considering the symmetry of stress distribution, the specimen is divided into 1200 elements for half-width as shown in Fig. 3. 11 and elastic FEM for plane

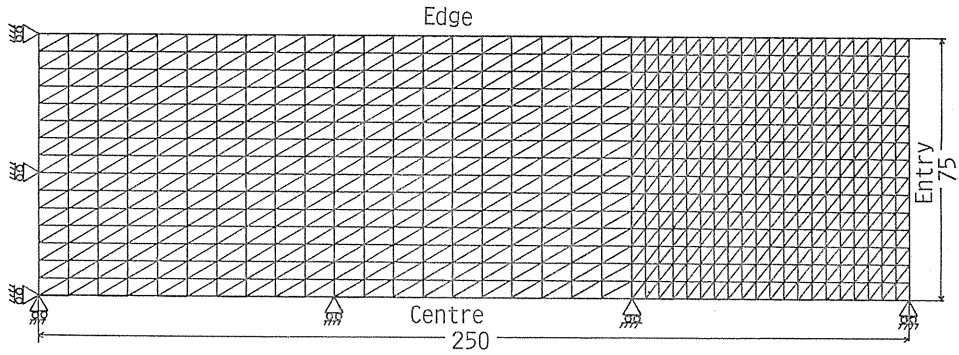

Fig. 3. 11 Finite mesh used for the analysis.

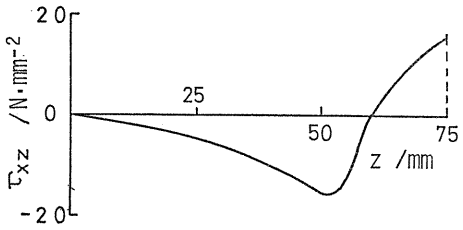

Fig. 3. 12 Distribution of transverse shearing stress at the entry of roll gap.

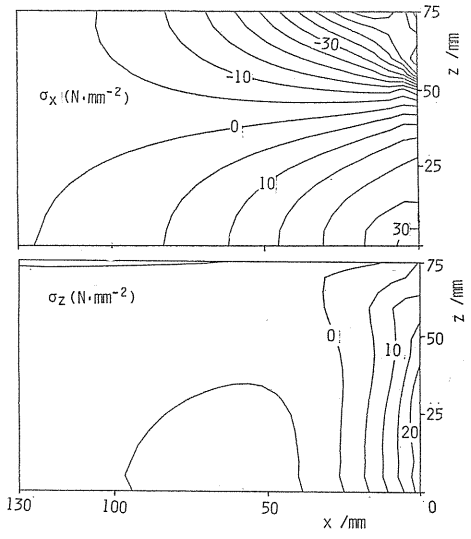

Fig. 3. 13 Distributions of normal stresses at the upper stream side of roll gap obtained by FEM.

stress condition is used. The distribution of longitudinal stress at the entry of roll gap obtained by the experimeut is used as a boundary condition. Besides, it is considered that the transverse shearing stress also acts on the boundary. But it is unknown, so the calculation is repeated by correcting the assumed distribution of transverse shearing stress until the calculated distribution of transverse stress at the entry agrees with experimental one.

Fig. 3. 12 shows the distribution of transverse shearing stress when the convergency is obtained. It is found that the region of negative spread in width direction exists near the centre of strip width and it is wider than the spread region. This tendency agrees with the calculated result obtained by the three-dimensional analysis[33]. Fig. 3. 13 shows the calculated result for the distributions of normal stresses at the upper stream side of roll gap. It agrees well with the experimental result (Fig. 3. 3).

Therefore it is made clear that the distribution of stresses at the upper stream side of roll gap is decided by the longitudinal stress and transverse shearing stress acted on the entry of roll gap. By utilizing the result the stresses at the entry of roll gap are estimated from the stress distribution at the upper stream side of roll gap.

3. 5. Conclusions

The distributions of strains at the upper stream side of roll gap during rolling are measured and the stresses are calculated from them. Then the stresses at there are discussed by comparing with the calculated result by FEM.

(1) Stresses occurs far away from the entry of roll gap and the position of its appearance is affected especially by strip width.

(2) The distributions of stresses at the upper stream side of roll gap change with reduction and strip width but not with front-tension.

(3) The transverse stress is not affected by back-tension, but the longitudinal stress is shifted to tensile side and the difference between the maximum stress and the minimum stress decreases with the increase of back-tension.

(4) It is made clear from the analysis by elastic FEM that the distribution of stresses at the upper stream side of roll gap is decided by not only the longitudinal stress but the transverse shearing stress at the entry of roll gap. By utilizing the result the stresses at the entry of roll gap are estimated from the stress distirbution at the upper stream side of roll gap.

Nomenclatures

x : rolling direction
y : vertical direction
z : transverse direction
σ_x, σ_y, σ_z, τ_{xz} : components of normal stress and shearing stress
ε_x, ε_y, ε_z, γ_{xz} : components of normal strain and shearing strain
p : rolling pressure $(=-\sigma_y)$
p' : rolling force per unit width
q' : contact force per unit width between backup roll and work roll
h, b : thickness and width of strip
δ : deflection of roll

δ_c : roll crown
r : reduction in thickness
σ_f, σ_b : front- and back-tension
ν, E, G : Poisson's ratio, Young's modulus and shear modulus of roll
A, I : cross-sectional area and moment of inertia of area of roll
$2L$: distance between the centres of bearings of roll
$2l$: length of roll barrel
l_d : length of the arc of contact
c : elastic constant assumed in local compression between cylinders
Δ : change in the distance between axes of two cylinders in contact
Ψ : projecting height of pin
p_p : detected load by pin

Subscripts

1, 2 : before and after rolling
B, W : backup roll and work roll
b, s, f : bending moment, shearing force and flattening

References

1) Tozawa, Y. et al.: J. Jap. Soc. Tech. Plasticity, 11-108 (1970), 29.
2) Tozawa, Y. et al.: J. Jap. Soc. Tech. Plasticity, 12-124 (1971), 337.
3) Tozawa, Y. et al.: J. Jap. Soc. Tech. Plasticity, 16-168 (1975), 52.
4) Tozawa, Y. et al.: J. Jap. Soc. Tech. Plasticity, 16-171 (1975), 345.
5) Kato, T. et al.: J. Jap. Soc. Tech. Plasticity, 21-236 (1980), 800.
6) Tozawa, Y. et al.: J. Jap. Soc. Tech. Plasticity, 21-238 (1980), 999.
7) Ishikawa, T. et al.: J. Jap. Soc. Tech. Plasticity, 22-247 (1981), 816.
8) Tozawa, Y. et al.: J. Jap. Soc. Tech. Plasticity, 22-249 (1981), 1030.
9) Tozawa, Y. et al.: Proc. 34th Jap. Joint Confer. for Tech. Plasticity, (1979), 49.
10) Emicke, O.: Stahl u. Eisen, 58 (1938), 73.
11) Larke, E. C.: The Rolling of Strip, Sheet and Plate, Chapman & Hall (1957).
12) Hichcock, J. H.: Roll Neck Bearings, ASME Research Pub. (1935).
13) Fujisawa, et al.: J. Jap. Soc. Tech. Plasticity, 16-171 (1975), 345.
14) Huggins, P. J. G.: J. Inst. Metals, 94 (1966), 238.
15) Fazan, B.: Revue de Metallurgie, 57-11 (1960), 1003.
16) Stone, M. D. et al.: Iron and Steel Engr., 42-8 (1965), 73.
17) Troost, A. et al.: Archiv für das Eisenhw., 37 (1966), 935.
18) Shiozaki, H.: J. Jap. Soc. Tech. Plasticity, 9-88 (1968), 315.
19) Tozawa, Y. et al.: Numerical Methods in Industrial Forming Processes, Ed. by Pittman, J. F. T. et al., Pineridge Press, Swansea (1982), 787.
20) Timoshenko, S.: Strength of Materials Part-Ⅱ, D. van Nostrand Company, Inc., New York, 1956.
21) Timoshenko, S. et al.: Theory of Elasticity, McGraw-Hill, New York, 1951.
22) Siebel, E., & Lueg, W.: Mitt. Kais. Wilh. Inst. Eisenf., 15 (1933), 1.
23) McGregor, C. W. et al.: J. of Applied Mechanics, 15 (1948), 297.
24) Smith, C. T., et al.: J. Iron & Steel Inst., 170 (1952), 347.
25) van Rooyen, G. T., et al.: J. Iron & Steel Inst., 186 (1957), 235.
26) Gokyu, I., et al.: J. Jap. Soc. Tech. Plasticity, 3-13 (1962), 73.
27) Matsuura, Y. & Motomura, M.: J. Jap. Soc. Tech. Plasticity, 9-86 (1968), 168.
28) Matsuura, Y., et al.: J. Jap. Soc. Tech. Plasticity, 10-102 (1969), 535.
29) Matsuura, Y., et al.: J. Jap. Soc. Tech. Plasticity, 11-116 (1970), 661.

30) Vater, M., et al.: Stahl u. Eisen, 86 (1966), 710.
31) Matsuura, Y., et al.,: J. Jap. Soc. Tech. Plasticity, 12-126 (1971), 529.
32) Tozawa, Y.: Advance Technology of Plasticity, Vol. 2 (1984), 1151.
33) Tozawa, Y., et al.: J. Jap. Soc. Tech. Plasticity, 23-263 (1982), 1181.